UNIVERSIDAD DE CHILE
FACULTAD DE CIENCIAS FÍSICAS Y MATEMÁTICAS
DEPARTAMENTO DE INGENIERÍA CIVIL

# RELACIONES ENTRE EL NIÑO – OSCILACIÓN DEL SUR Y RESPUESTA HIDROLÓGICA EN CHILE CENTRO-SUR

MEMORIA PARA OPTAR AL TÍTULO DE INGENIERO CIVIL

DIEGO ALBERTO HERNÁNDEZ NEIRA

PROFESOR GUÍA:
PABLO MENDOZA ZÚÑIGA

MIEMBROS DE LA COMISIÓN:
FRANCO RICCHETTI CAMPOS
XIMENA VARGAS MESA

SANTIAGO DE CHILE
2020

**RESUMEN DE LA MEMORIA PARA OPTAR AL TÍTULO DE**: Ingeniero Civil

**POR**: Diego Alberto Hernández Neira

**FECHA**: 20/07/2020

**PROFESOR GUÍA**: Pablo Mendoza Zúñiga

# RELACIONES ENTRE EL NIÑO – OSCILACIÓN DEL SUR Y RESPUESTA HIDROLÓGICA EN CHILE CENTRO-SUR

Si bien existe evidencia de teleconexiones entre El Niño Oscilación del Sur (ENOS) y la hidroclimatología de la zona centro-sur de Chile, no es todavía clara la propagación de la señal ENOS a través del ciclo hidrológico, debido a efectos complejos de los procesos hidrológicos que podrían compensar o amplificar las anomalías meteorológicas. En este trabajo se examina la respuesta hidrológica a las fases de ENOS, manifestadas como fluctuaciones en las condiciones climáticas locales, a lo largo de 54 cuencas de estudio en régimen cercano al natural. El dominio de estudio provee un marcado gradiente hidroclimático latitudinal, además del control altitudinal causado por la Cordillera de Los Andes. Se analiza la dependencia de variables climáticas e índices hidrológicos de acuerdo a las fases de ENOS – El Niño, La Niña y neutral –, en distintos regímenes hidrológicos – nival, pluvial y mixto. Además, se calcula la sensibilidad de los índices hidrológicos a las variables climáticas, y de esta forma, los patrones obtenidos para las sensibilidades empíricas son claves con miras a intentar separar el efecto individual de las fluctuaciones en precipitación y temperatura inducidas por ENSO, dentro del efecto integrado o total de ENOS sobre el ciclo hidrológico.

Los resultados obtenidos confirman significancia estadística en las anomalías inducidas por ENOS sobre caudales y/o variables climáticas a escala de cuenca, en toda la zona de estudio. Los regímenes hidrológicos (i.e., estacionalidad) son exacerbados durante la fase El Niño, con un claro gradiente latitudinal. Se observa una estacionalidad distintiva de las anomalías de temperatura según ENOS, con condiciones más cálidas (más frías) en invierno y más frías (más cálidas) en primavera durante la fase El Niño (La Niña), presumiendo efectos dispares sobre el comportamiento de la nieve y caudales. Se observa concurrencia entre condiciones húmedas (secas) y menores (mayores) coeficientes de escorrentía, en cuencas de régimen nival. De esta manera, en cuencas nivales se observan relaciones compensatorias que impactan la respuesta de caudal. Finalmente, se busca desagregar los efectos de precipitación y temperatura modulados por ENSO, estimando que el rol de la temperatura es secundario frente a la precipitación pero no despreciable, y que este efecto es de signo distinto para cuencas nivales o pluviales.

Esta memoria se presenta en idioma inglés y en formato tipo artículo de revista.

## *Linking ENSO teleconnections and hydrological responses in Central-Southern Chile: a climate sensitivity approach*

# ABSTRACT

Despite large evidence on teleconnections between the El Niño Southern Oscillation (ENSO) and the hydroclimatology of Central-Southern Chile, the propagation of the ENSO signal through the hydrological cycle is still unclear, because of the complex hydrological processes and compensatory/amplifying effects of meteorological anomalies on the hydrology. In this work, we examine the hydrological responses to contrasting ENSO phases, which manifest as fluctuations in local climatic conditions across 54 near-natural catchments, whose location provides a strong north-south latitudinal dry-wet gradient, with the Andes Cordillera acting as a longitudinal elevation control. We analyze the dependence of climatic variables and hydrological signatures according to ENSO phases – El Niño, La Niña and neutral – across different hydrologic regimes – snowmelt-dominated, rainfall-dominated and mixed. Additionally, we calculate the sensitivity of hydrological signatures to climatic variables. Here, the patterns of empirical sensitivities are valuable keys in order to attempt to unravel the integrated effect of ENSO-related precipitation and seasonal temperatures fluctuations over the water cycle.

Our results confirm statistically significant ENSO-related anomalies of streamflow and/or catchment-scale climatic variables in all basins within the domain. Hydrologic regimes (i.e. seasonality) are enhanced during El Niño years, showing a clear latitudinal gradient. We observe a distinct temperature timing according to ENSO, with warming (cooling) in winter and cooling (warming) in spring during El Niño (La Niña) events, with presumable uneven effects over snow behavior and streamflow. We note concomitancy between wetter (drier) conditions and lower (higher) runoff ratios in snowmelt-driven basins. Thus, for snowy catchments, we account compensatory relationships that buffer streamflow. Finally, we attempt to disaggregate the effects of ENSO-related precipitation and temperatures fluctuations on overall streamflow response, roughly estimating that temperature role is not negligible nor univocal.

*A mi abuelo Carlos*

*A mi familia*

*“*

*Y una respuesta sin pregunta*
*es como un rey sin corona…*

*¿quién posee la verdad*
*si no la Naturaleza?,*
*¿el aire, el agua, el fuego, la tierra?*

*”*

*Makiza (1999). Aerolíneas Makiza.*

# AGRADECIMIENTOS

En el contexto en el cual ocurre esta titulación, cobra especial sentido valorar más que nunca la simple y pura compañía de quienes me han apoyado durante estos años. Este texto cierra un proceso de ya varios años, y al final, no podría hacer otra cosa sino agradecer.

A lxs profesorxs por enseñarme todo lo que sé y semillar lo que se habrá de inventar, y por la motivación tremenda con que nos acercan a este futuro-ya-presente. Especialmente a mis profesores de comisión… A la profesora Ximena por ser una referente imbatible. A Franco por su comprensión, consejos y punto de vista. A Pablo, por el tiempo dedicado (¿qué más valioso?), por la motivación gigante, confianza y buena onda. También agradezco a los profesores con quienes he tenido la oportunidad de trabajar juntos: Miguel, Pablo, Franco, profe Ximena y profe James, de quienes atesoro mucho los aprendizajes recibidos.

Agradezco a mi madre Carola, por sus palabras y por ser tan distintos. A mi padre Carlos, por la confianza y por ser tan parecidos. A mi hermana Ignacia por la complicidad. A mis abuelos Rosa y Jaime por el cariño y las risas. A mi abuela Elsa a quien admiro y me inspira un montón. A mi familia en general, por el cariño que he recibido desde siempre.

A mis amigxs del colegio, con quienes llevamos media vida juntos y es difícil saber dónde termina uno y dónde empieza el otro. Por la calidez, el amor, y la forma de ver las cosas.

A mis amigxs de la U desde plan común, por ‘chapotear’ juntos este ya-no-tan-extraño Bochef. Por el terraceo habitual (punto fijo los sábados…) de los primeros años. Por habernos hecho sentir acompañados y haber disfrutado, y porque siempre es un gusto compartir con ustedes, me siento muy afortunado.

A mis compañerxs de la U en general, de quienes he recibido muchas veces solidaridad y ayuda desinteresada. A mis amigxs y compañerxs de Civil, agradezco al tremendo grupo. Egreso de esta facultad con una excelente vivencia, de empatía, de amabilidad, de muchas personas que intentan aportar a lo que les parece que se debe hacer mejor.

Dedico este trabajo especialmente a mi abuelo Carlos, por haber estado siempre tan interesado en cómo me iba en la U. De sus palabras obtuve el valor del esfuerzo, y de sus acciones recibí el valor del cariño. He tenido la suerte de toparme con grandes personas a quienes sería injusto dejar fuera, y agradezco a todos de quienes he obtenido aprendizajes.

# TABLA DE CONTENIDO

# ÍNDICE DE TABLAS

# ÍNDICE DE FIGURAS

# 1 INTRODUCTION

Hydrology along Central-Southern Chile is modulated by contributions of several modes of natural variability – as El Niño Southern Oscillation (ENSO), Pacific Decadal Oscillation and Antarctic Oscillation – with notable influence of ENSO over winter and annual hydrology-related variability (Rubio-Álvarez and McPhee, 2010). Ultimately, ENSO represents the paramount fluctuation in the global climate-system variability at the year-to-year scale (Timmerman et al., 2018; Grothe et al., 2020). Timmerman et al. (2018) reviewed the current understanding about the complexity of the ENSO phenomenon, identifying dynamics with a low-frequency mechanism during boreal spring – enough warming of Central Pacific pool – and a stochastic activation mechanism during boreal summer – westerly wind events – related to momentum transfer. The interaction between both mechanisms determines the apparition of “El Niño” phase or the opposite “La Niña” phase. It is worth noting that both phases are not symmetrical: while often El Niño phases are stronger than La Niña (larger amplitude of sea surface temperature anomalies), La Niña phases show greater persistence in time than El Niño (year-to-year consecutive occurrence), besides others nonlinear features. Despite ENSO manifests itself as an multi/interannual climate fluctuation, its causes are related to interactions of mechanisms that cover a myriad range of processes in temporal scales from weeks to decades (Timmerman et al., 2018).

ENSO fluctuations determine pseudo-oscillatory perturbations in sea surface temperature and winds, which affect the general circulation of atmosphere-ocean and climate of vast regions around the globe, as Asia, America and Australia. The ENSO phenomenon must be understood as a continuum between El Niño and La Niña phases, subject to asymmetry and nonlinearity, where there are no events with identical manifestation (Timmerman et al., 2018) – with sometimes notable uneven evolution of El Niño events (e.g., Hu and Fedorov, 2016; Min et al., 2015). ENSO events may be classified as strong, moderate and weak, according to their amplitudes of sea surface temperature anomalies. Even more, at least two spatial characteristic configurations can be identified in El Niño-phase events (i.e., “flavors”), since some events show major warming towards the East Pacific region, or major warming through the Central Pacific region (Timmerman et al., 2018).

ENSO has also been recognized as an important control over Central-Southern Chile hydroclimatology. Waylen et al. (1993) reported positive, statistically significant annual precipitation anomalies during El Niño years across fifteen stations between 27°S and 38°S, located in basins within a wide range of hydrologic regimes. Montecinos and Aceituno (2003) analyzed the ENSO-related variability of precipitation in Central Chile for the second half of 20th century. They found that El Niño (La Niña) episodes can be associated to: above (below) average winter precipitation for the region between 30°S to 35°S, above (below) average late spring precipitation in the region from 35°S to 38°S, and dry (humid) conditions during summer for the 38°S to 41°S region, showing larger amplitude the two first relationships mentioned above. The synoptic pattern of El Niño-related precipitation anomalies indicates blocking activity over the Amundsen-Bellingshausen Seas that forces to northward deviation of track-of-storms in the South East Pacific (Montecinos and Aceituno, 2003).

Nevertheless, hydrological response to ENSO fluctuations is not alleged to mimic ENSO-related precipitation anomalies, due to further complexity related to catchment processes and dependence on other variables such as temperature. Cortés et al. (2011) identified a subregion within 30°S to 34°S where timing of streamflow (seasonality) is controlled by winter and spring temperature besides annual precipitation. During El Niño years, increased temperature and greater precipitation amounts seem to have compensatory effects on streamflow seasonality, making it difficult to recognize the overall effect of El Niño episodes. Greater snowpack accumulation is observed during El Niño years, although the opposite is not clear during La Niña events, as reported by Masiokas et al. (2006) within region spanning 30°S to 37°S and by Cortés and Margulis (2017) for the domain 27°S to 37°S, suggesting that a nonlinear modulation of ENSO phases on hydrological variables exists. Further assessments of the effects that precipitation and temperature anomalies have on hydrological responses are needed.

Several approaches have been explored to assess water resources sensitivities to climate variability and change, including: empirical nonparametric-based techniques to characterize regional patterns of streamflow response and dependencies with storage processes and other factors (Sankarasubramanian and Vogel, 2003; Sankarasubramanian et al., 2001); multi-model frameworks to assess structural uncertainties in hydrologic responses to climate shifts (Vano et al., 2012); empirical regression-based techniques to explore implications of solid partition of precipitation in anomalies of streamflow (Berghuijs et al., 2014); Budyko frameworks to globally assess the dominance of precipitation temporal variability on streamflow (Berghuijs et al., 2017), and to better understand effects of temperature on evaporation and radiation feedbacks over streamflow (Milly et al., 2018); radiation parameterizations to assess albedo losses importance on streamflow anomalies due to warming (Milly and Dunne, 2020); and empirical methods fed with climate projections to constrain streamflow projections (Lehner et al., 2019).

However, the interpretation of sensitivity calculations is challenging because they depend on the conceptualization of basin function. Hence, estimated sensitivities may not be numerically comparable between different studies. Moreover, the sensitivities depend on the historical period and length of recorded data (Sankarasubramanian et al., 2001), as well as measurement errors, temporal and spatial sampling errors that may undermine the true value of sensitivities (Milly et al., 2018). It may be worth noting that some formulations of sensitivities lay on imposition of an arbitrary change of a climatic variable. Likewise, as noted by Berghuijs et al. (2017), sensitivities by itself do not provide the observed (historical) magnitude of change of a climatic variable, but the degree of response to a reference change.

We relate hydrologic sensitivities to climatic variables to assess the compounded influence of ENSO on water resources. To our knowledge, the disentangled effects of ENSO-related precipitation and temperature anomalies on the water cycle in Central-Southern Chile has not been achieved. This work explores the main patterns of ENSO modulation over climatic variables and hydrological signatures, and aims to separate ENSO-related intra-seasonal temperature signal and its implications. Hence, we explore hydrological sensitivities to climate over Central-Southern Chile, to roughly identify the individual effect of each climatic ENSO-anomaly on hydrological anomalies. We present our results based on a hydrologic regime classification, in order to frame our findings and implications around sub-regions with similar hydrologic behavior. Therefore, our main goals are:

i. To identify and describe observed ENSO-related anomalies in the water cycle, with special focus on sub-regional patterns.
ii. To link observed climate sensitivities on the study domain with plausible hypothesis reported on literature.
iii. To unravel the individual roles of precipitation and temperature inside the integrated effect of ENSO anomalies over the hydrology.

# 2 STUDY DOMAIN

The study area spans the region between 28°S and 41°S in Central-Southern Chile, which is bounded by the Pacific Ocean in the west, and by the Andes Cordillera in the east. Further north from the study domain, around 27°S offshore, the Southerneast Pacific Anticyclone blocks precipitation events boosting a strong north-south latitudinal dry-wet gradient. Further, the Andes Cordillera acts as a longitudinal elevation control, with peak elevation above 6500 m a.s.l. in the study domain (Table 1 and Figure 1). Most precipitation events along this territory are associated with frontal systems, which landfall in winter between 30°S and 40°S (subtropical), and during the entire year between 40°S and 55°S (midlatitude). Atmospheric rivers landfalling against the Andes Cordillera are an important feature that contribute nearby more than half of annual precipitation in subtropical and midlatitude Chile, whose intensity may reach up to two or three times compared to other storms due to the orographic enhancement of precipitation (Viale et al., 2018).

Central-Southern Chile concentrates the most populated cities in the country, including the capital Santiago, and key water-intensive activities such as as mining, agriculture and forest plantations (DGA, 2016). Climate in this region is mainly Mediterranean-like, from cold semiarid climate at the north of the study domain, to temperate rain-oceanic climate at southmost, passing through subhumid and humid Mediterranean climates (Alvarez-Garreton et al., 2018).

*Table 1. Main physiographic characteristics of the basins at the study domain, according to hydrologic regime classification.*

| Basins | Latitude of gauge (°S)<br>Minimum<br>Median<br>Maximum | Longitude of gauge (°W)<br>Minimum<br>Median<br>Maximum | Mean elevation (m a.s.l.)<br>Minimum<br>Median<br>Maximum | Peak elevation (m a.s.l.)<br>Minimum<br>Median<br>Maximum | Area ($km^2$)<br>Minimum<br>Median<br>Maximum | Average slope (%)<br>Minimum<br>Median<br>Maximum |
|---|---|---|---|---|---|---|
| Snowmelt-driven (n = 12) | 28.09<br>32.41<br>35.28 | 71.02<br>70.45<br>69.94 | 1,973<br>3,303<br>3,905 | 3,282<br>5,486<br>6,550 | 110<br>777<br>4,839 | 19.6<br>23.8<br>29.6 |
| Mixed (n = 17) | 30.44<br>32.92<br>39.26 | 72.23<br>70.87<br>70.54 | 206<br>1,857<br>2,726 | 833<br>3,591<br>5,539 | 56<br>559<br>1,837 | 12.3<br>22.2<br>25.6 |
| Rainfall-driven (n = 25) | 33.17<br>37.78<br>40.71 | 73.23<br>72.44<br>71.13 | 152<br>504<br>1,564 | 588<br>1,510<br>3,509 | 103<br>688<br>4,510 | 6.6<br>12.6<br>25.9 |

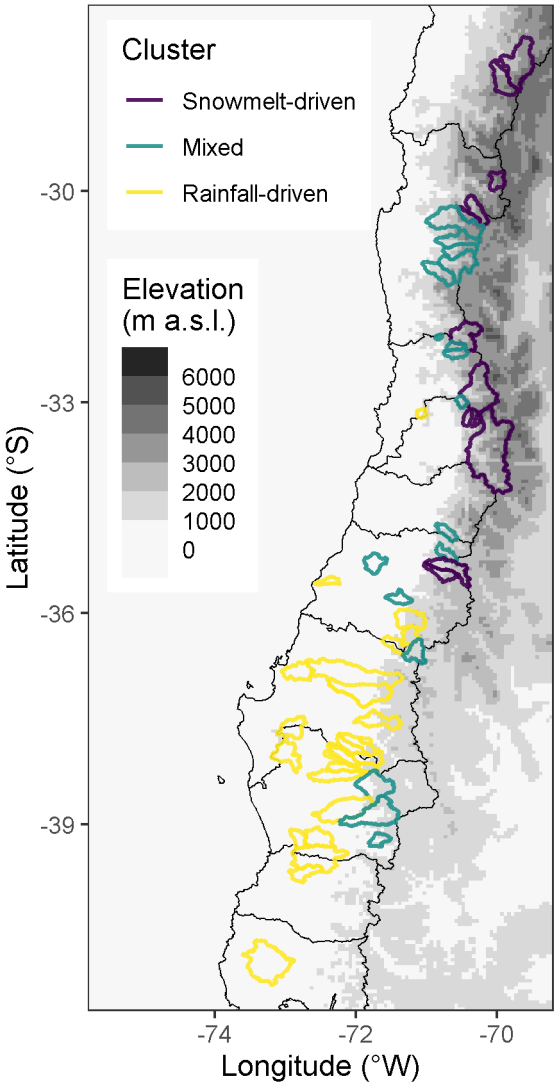


*Figure 1. Location, elevation and hydrologic regime of basins across the study domain.*

# 3 DATA AND METHODS

## 3.1 Datasets

We use the CAMELS-CL basin-scale dataset (Alvarez-Garreton et al., 2018), which contains daily time series of streamflow, precipitation, temperature and other hydrometeorological variables. The streamflow time series correspond to observed records collected in stations from the National Water Directorate (*Dirección General de Aguas*, DGA). Precipitation and temperature time series in CAMELS-CL are obtained from the CR2MET gridded product (http://www.cr2.cl/datos-productos-grillados/), which is already calibrated with DGA and National Weather Directorate *(Dirección Meteorológica de Chile*, DMC) observations.

The study period is 1979-2015, i.e., 36 water years, defined from April 1$^{st}$ to March 31$^{st}$. From all basins available in the CAMELS-CL dataset, 103 are classified as near-natural regime non-nested catchments, according to givens water rights criteria – consumptive water rights smaller than 5% of mean annual streamflow – and absence of dams (DGA, 2019a). Based on quality criteria, we select 54 basins for further analyses.

While the meteorological times series are complete, daily streamflow time series have missing values. Hence, we define four quality control steps for streamflow data to include a specific basin into our analyses:

i. A monthly value is considered missing if it contains more than 20% of daily missing values.
ii. An annual value is considered missing if it contains more than two monthly missing values.
iii. We select a basin if it has at least 15 years of data (not necessarily consecutive); and,
iv. we select a basin if it does not contain a 10-year gap of data.

After applying the above constraints, we obtained 54 near-natural basins containing 87.5% of daily streamflow data. We fill the missing data at the monthly time scale using the imputePCA R package (Josse and Husson, 2016), which consists of iterative Principal Component Analysis imputation, taking advantage of structures between individuals (i.e., months along years) and structures between variables (i.e., basins). We conduct imputation stratified per month, and we perform a similar procedure at the daily time step before compute flow duration curves (FDC).

## 3.2 Seasonality of streamflow and precipitation

We calculate monthly Pardé coefficients of streamflow (e.g., Blöschl et al., 2013), for each water year. The Pardé coefficient is defined as the quotient of monthly streamflow over the corresponding annual streamflow (for each basin, twelve values per year). For simplicity, Pardé coefficients are scaled so that monthly values sum the unity for each water year, thus coefficients range from 0 to 1 (referred as fractional coefficients in later text). Additionally, we calculate identical coefficients for precipitation.

At each basin, we calculate the averaged fractional coefficients for streamflow and use them as input variables for a K-means clustering procedure with fixed K=3, according to the well-known classification for hydrologic regimes: rainfall-driven, snowmelt-driven and mixed regimes. We also explore the inclusion of a precipitation-based Pardé coefficient as clustering variable, which forces to an attenuation or suppression of the number of mixed regime basins, strengthening the classification to snowmelt-driven and rainfall-driven clusters (not shown). Therefore, we decide to keep catchment classification using only streamflow data. We also performed K-means clustering based on the mean centroid of the annual hydrograph, with little differences but slightly lesser coherent spatial patterns (not shown). Finally, we confirm the results of the classification process by individual inspection of seasonal streamflow curves at each basin (supplementary Figure B-1).

## 3.3 ENSO type of year classification

Past studies suggest that, because of ENSO complexities, each event is unique, and hence ENSO episodes should be interpreted as a continuum instead of strictly defined phases (e.g., Timmermann et al., 2018; Hu and Fedorov, 2016; Min et al., 2015). Notwithstanding, in this study we classify a year as El Niño, La Niña or neutral at the annual scale, according to the annual average Multivariate ENSO Index (MEI; Wolter and Timlin, 2011; https://www.esrl.noaa.gov/psd/enso/mei). MEI is one of most comprehensive ENSO indexes, based on Principal Components Analysis of five fields over the tropical Pacific basin. We define an El Niño year when the median MEI value is equal or larger than 0.5, a La Niña year when it is equal or smaller than -0.5, and neutral otherwise (supplementary Figure B-2). We compare this numerical criterion with previously published lists of ENSO events comprehensive classification (Yu and Kim, 2013; Zheng and Yu, 2017), finding high correspondence with our results.

## 3.4 Flow duration curves

For each basin and water year, we calculate the FDC with the daily streamflow normalized with the corresponding average daily streamflow (e.g. Yokoo and Sivapalan, 2011; Yaeger et al., 2012; Chouaib et al., 2018), in order to harmonize the effects of spatial variability and achieve comparable metrics between different catchments.

When we aggregate annual FDC within a hydrologic regime cluster and within an ENSO phase, we calculate a mean annual FDC instead of a total-record FDC, according to McMillan et al. (2017) who emphasizes the more robustness of mean FDC, due the length-of-data dependence of total-record FDC.

## 3.5 Climatic variables and hydrological signatures

In order to visualize the main effects of ENSO phases on the hydrological cycle, we select four climatic variables and four hydrological signatures (Table 2). Because of the large climate variability along the Chilean territory, we define a six-month winter season (April-September) that encompasses 70% to 95% of annual precipitation, in mean terms, at the different basins. Additionally, we define a three-month spring season (October-December). The remaining three-months summer are disregarded from our analyses, because of lack of statistical significance in January-March temperature anomalies according to ENSO phases (not shown).

We define a winter precipitation event (or storm) when daily precipitation is larger than a 2 mm threshold at any day during winter (April-September). Although 2 mm is a small threshold, we consider it appropriate because of the catchment-scale analyses, and also due to undercatch or underestimation issues on both observations and reanalyses datasets across the territory (DGA, 2019b; Beck et al., 2019). Further, an arbitrary threshold is needed because near to zero values may be produced by numerical artifacts of the gridded-product and because of catchment-scale averaging.

We select a suite of hydrological signatures to cover distinct aspects of the hydrological cycle. The runoff ratio ($\boldsymbol{RR}$) may be interpreted as water yield efficiency, while the centroid of annual hydrograph ($\boldsymbol{CEN}$) is used as indicator of streamflow seasonality (e.g. Cortés et al., 2011). In addition, the low-segment volume of the flow duration curve ($\boldsymbol{LOWV}$; Yilmaz et al., 2008) is proposed as an alternative baseflow index (McMillan, 2019).

*Table 2. Annual time series of climatic variables or hydrological signatures, for each basin.*

| Type | Name | Description | Units |
|---|---|---|---|
| Climatic variable | Cumulative precipitation of winter storm events ($\boldsymbol{PR_{sto}}$) | For each water year, cumulative precipitation of daily winter precipitation events (as defined in text), normalized over long-term mean. | % |
| Climatic variable | Mean temperature of winter storm events ($\boldsymbol{TM_{sto}}$) | For each water year, mean air temperature of daily winter precipitation events (as defined in text). | °C |
| Climatic variable | Mean temperature of winter days ($\boldsymbol{TM_{win}}$) | For each water year, mean air temperature of winter days (April-September) | °C |
| Climatic variable | Mean temperature of spring days ($\boldsymbol{TM_{spr}}$) | For each water year, mean air temperature of spring days (October-December) | °C |
| Hydrological signature | Streamflow ($\boldsymbol{Q}$) | For each water year, annual streamflow, normalized over long-term mean. | % |
| Hydrological signature | Runoff ratio ($\boldsymbol{RR}$) | For each water year, annual streamflow over annual accumulated precipitation. | % |
| Hydrological signature | Centroid of annual hydrograph ($\boldsymbol{CEN}$) | For each water year, center of mass of the daily streamflow record (Cortés et al., 2011). | weeks |
| Hydrological signature | Low-segment volume of Flow Duration Curve ($\boldsymbol{LOWV}$) | For each water year, volume of the flow duration curve on semi log space, between exceedance probabilities 0.7 and 1.0 (Yilmaz et al., 2008). | units |

## 3.6 Composites and grouping

We compute composites of climatic variables and hydrological signatures (see Table 2) related to ENSO anomalies, as follows. For each basin and variable, the long-term mean is subtracted from the annual time series obtaining the anomalies time series,

$$Anomalies\ of\ z := z'_t = z_t - \bar{z}$$

where $z_t$ is either a climatic variable or hydrological signature annual time series, and $\bar{z}$ is its mean. Then, composites are calculated as the average of annual anomalies from all years within a certain ENSO phase – El Niño, neutral or La Niña. A special composite is calculated as the average of annual anomalies of all years classified as El Niño minus the average of annual anomalies of all years classified as La Niña. This way, the latter composite indicates in a single term the amplitude or how much the analyzed variable shifts according to ENSO phenomenon – in mean terms.

$$Composite_{El\ Niño}\ of\ z := \underset{t\ \epsilon\ \{El\ Niño\}}{mean}(z'_t)$$

$$Composite_{Neutral}\ of\ z := \underset{t\ \epsilon\ \{Neutral\}}{mean}(z'_t)$$

$$Composite_{La\ Niña}\ of\ z := \underset{t\ \epsilon\ \{La\ Niña\}}{mean}(z'_t)$$

$$Composite_{El\ Niño-La\ Niña}\ of\ z := \underset{t\ \epsilon\ \{El\ Niño\}}{mean}(z'_t) - \underset{t\ \epsilon\ \{La\ Niña\}}{mean}(z'_t)$$

For time series composites of El Niño minus La Niña phases at every basin, we conduct a Fisher-Pitman permutation test to check the statistical significance of such differences, where the null hypothesis establishes that there is no difference (equal to zero) between means. This test is computed at the 95% significance level.

We also perform a Wilcoxon (or Mann-Whitney) nonparametric test to assess the difference between annual time series grouped by: (i) ENSO-phases type of year (i.e., temporal grouping), and (ii) hydrologic regime clusters (i.e., spatial grouping). The Wilcoxon test lays on the null hypothesis that there is no difference between group means. This test is computed at the 95% significance level.

## 3.7 Hydrologic sensitivities

In particular, streamflow sensitivity to precipitation – typically referred to as elasticity – is defined as the fractional change in streamflow due to a fractional, long-term change in precipitation (e.g. 1% of change in precipitation, so elasticity has units of $\%\%^{-1}$). Sensitivity to temperature is analogous, but accounting an absolute change in temperature (e.g. 1°C of change in temperature, so sensitivity has units of $\%°C^{-1}$).

We compute sensitivities of two hydrological signatures – $\boldsymbol{Q}$ and $\boldsymbol{RR}$ – against the four climatic variables, for each basin at the annual scale. These sensitivities are calculated assuming that each signature can be represented in a multiple linear model with the four climatic variables as the explanatory variables, extending the idea of Berghuijs et al. (2014). Also, due to correlations between climatic variables, we consider each climatic variable as a multiple linear model with the three remaining climatic variables as independent variables. This approach is convenient to attempt to correct multicollinearity between predictor variables.

Regardless of the linear dependence assumption, all models for $\boldsymbol{Q}$ are statistically significant at the F-test (at 95% level of significance; supplementary Table B-1). Also for $\boldsymbol{Q}$, all models are statistically significant at the t-test for $\boldsymbol{PR_{sto}}$ as predictor (at 95% level of significance; supplementary Table B-1). For the temperature variables as predictors, models show varied behavior of t-test significance by basin (supplementary Table B-1).

Although regression-based climate sensitivities are typically computed using partial derivatives, this approximation may be quite unrealistic because they rely on the assumption that the values of the remaining variables are fixed, ignoring interactions and correlations between variables. Hence, we calculate sensitivities as the total derivative, as discussed in Berghuijs et al. (2017). For each basin, we resolve each sensitivity in a 4x4 linear system of equations, where the total derivatives are the unknowns and the partial derivatives are approximated by least squares as the coefficients of regression of the multiple linear models. Thereby,

$$Sensitivity\ of\ y_i\ to\ x_j := \frac{dy_i}{dx_j} = \frac{\partial y_i}{\partial x_j} + \sum_{k \neq j} \frac{\partial y_i}{\partial x_k} \cdot \frac{dx_k}{dx_j}$$

$$with\ \frac{dx_k}{dx_j} = \frac{\partial x_k}{\partial x_j} + \sum_{l \neq \{k,j\}} \frac{\partial x_k}{\partial x_l} \cdot \frac{dx_l}{dx_j}$$

where $y_i$ is a hydrological signature, $x_j$ is a predictor climatic variable and $x_k$ are the remaining – three of the four – climatic variables. The explicit equations systems for $\boldsymbol{Q}$ and $\boldsymbol{RR}$ climate sensitivities are shown in Supplementary A.

In order to avoid the influence of outliers in the multiple linear regression models, we conduct the following steps in the model adjustment process: (i) after adjusting a first model, we remove predictand observations when they are not contained in the range of fitted values ± 1.96 units of standard error of the regression (i.e. 95% confidence interval assuming normality), then (ii) a second and definitive model is adjusted.

## 3.8 Weighted sensitivities

Due that sensitivities by their own do not provide a realistic range of variations of the predictor climatic variable, we weight sensitivities by a certain variation of the climatic variable, as follows,

$$Weighted\ sensitivity\ of\ y_i\ to\ x_j := \frac{dy_i}{dx_j} \cdot \Delta x_j$$

where $\Delta x_j$ is chosen as an observed amplitude of variation of the climatic variable $x_j$. In the following, we pick $\Delta x_j$ as the observed composite (El Niño minus La Niña) of $x_j$.This way, weighted sensitivities address the degree of response to the observed amplitude of ENSO-variation of $x_j$.

Furthermore, we add all weighted sensitivities of $\boldsymbol{Q}$ to climate to obtain a "reconstructed" ENSO-variation amplitude of $\boldsymbol{Q}$, in a linear-dependence basis (e.g., Lehner et al., 2019),

$$\delta Q := \sum_j \frac{dQ}{dx_j} \cdot \Delta x_j$$
$$= \frac{dQ}{dPR_{sto}} \cdot \Delta PR_{sto} + \frac{dQ}{dTM_{sto}} \cdot \Delta TM_{sto} + \frac{dQ}{dTM_{win}} \cdot \Delta TM_{win} + \frac{dQ}{dTM_{spr}} \cdot \Delta TM_{spr}$$

where $\delta Q$ is the – linear dependent – reconstructed amplitude of variation of $\boldsymbol{Q}$. As $\Delta x_j$ are chosen to be the observed composites (El Niño minus La Niña) of $x_j$, we contrast $\delta Q$ to the observed composite (El Niño minus La Niña) of $\boldsymbol{Q}$, attempting to decompose the ENSO-related anomalies of $\boldsymbol{Q}$ into the climate weighted sensitivities terms of $\delta Q$.

Finally, in order to address the ENSO-related disentanglement of precipitation-anomalies effects against temperature-anomalies effects, we calculate a simple ratio of precipitation effect over the overall ENSO-related streamflow variation.

$$Ratio := \left(\frac{dQ}{dPR_{sto}} \cdot \Delta PR_{sto}\right) / \delta Q$$

Values of ratio > 1 indicate that the overall streamflow response is less than the sole precipitation effect, so temperature effect is counterweighting. Values of ratio < 1 indicate that a part of the overall streamflow response is due to temperature effect, so precipitation and temperature effects are compounding.

# 4 RESULTS AND DISCUSSION

## 4.1 Inter-annual variability of climatic variables and hydrological signatures

Figure 2 and Figure 3 show standard deviation of climatic variables and hydrological signatures, respectively, in order to quantify their inter-annual variability within the study domain. $\boldsymbol{PR_{sto}}$ (Figure 2) and $\boldsymbol{Q}$ (Figure 3) are already normalized by long-term means (see Table 2), so the standard deviation for these variables match with the coefficient of variation of raw variables. Standard deviations of $\boldsymbol{PR_{sto}}$, $\boldsymbol{TM_{sto}}$ and $\boldsymbol{TM_{win}}$ show a clear latitudinal gradient (Figure 2), with notable high variability of $\boldsymbol{PR_{sto}}$ at northernmost of study domain. The latter is expected as annual precipitation amounts in northern basins are explained by just a few storms during the year. Regardless of latitudinal control, when grouping according to hydrologic regime classification we obtain mean within-cluster standard deviations of 66.3%, 49.5% and 23.5% for snowmelt-driven, mixed and rainfall-driven hydrologic regimes, respectively. $\boldsymbol{TM_{sto}}$ exhibit larger variability than $\boldsymbol{TM_{win}}$ trough all clusters (1.2°C, 1°C and 0.7°C; against 0.7°C, 0.7°C and 0.6°C; respectively), and mean $\boldsymbol{TM_{spr}}$ variability shows an inverse but less clear pattern than remaining climatic variables (0.6°C, 0.7°C and 0.7°C).

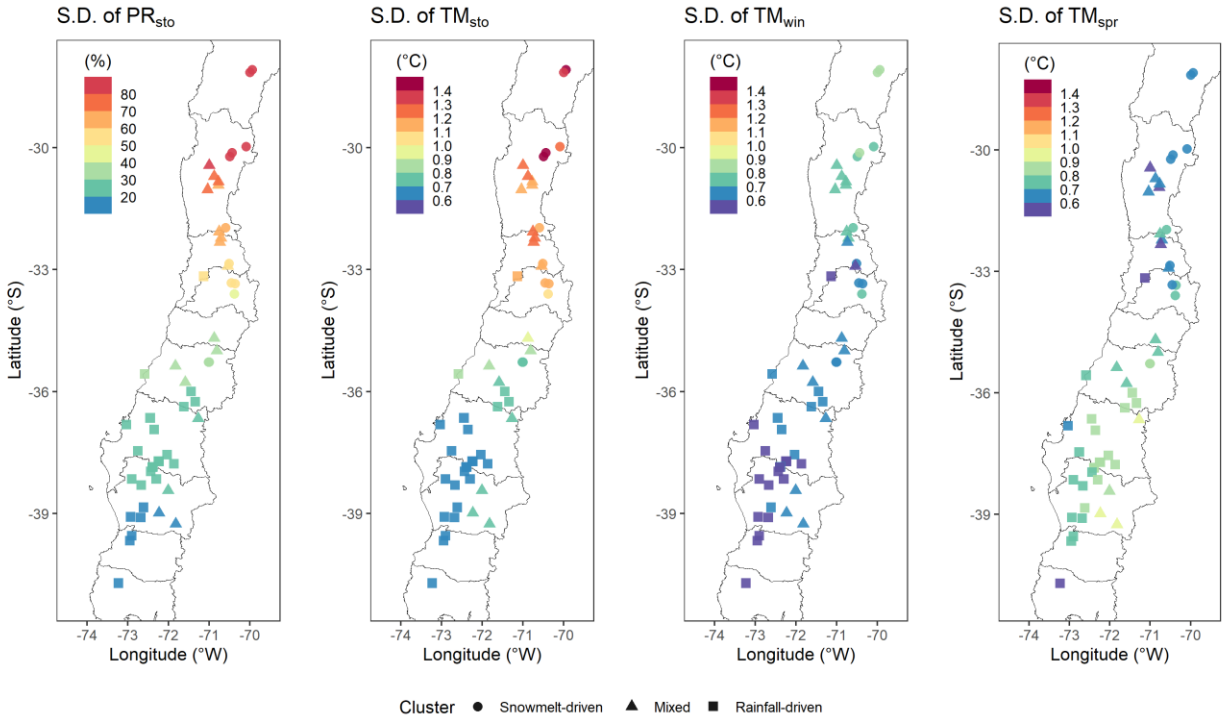


*Figure 2. Standard deviation for annual time series of climatic variables. Left to right: precipitation of winter storms, mean temperature of winter storms, mean temperature of winter, and mean temperature of springs, respectively.*

Figure 3 shows latitudinal variations for $\boldsymbol{Q}$, $\boldsymbol{RR}$ and $\boldsymbol{CEN}$. For $\boldsymbol{Q}$, the gradient-pattern at the northernmost sub-domain is slightly different than for precipitation, with superposition of precipitation variability pattern and basin attenuation effect. Therefore, $\boldsymbol{Q}$ variability is larger than $\boldsymbol{PR_{sto}}$ variability in most of basins (43 out of 54), excepting most of snowmelt-driven cluster (9 out of 12) and a few mixed basins (2 out of 17). This is consistent with runoff attenuation effects of snow storage, and elasticities larger than 1 across mixed and rainfall-driven basins. Averaged standard deviations for $\boldsymbol{Q}$ are 55.6%, 68.9% and 33.8% among snowmelt-driven, mixed and rainfall-driven catchments, respectively. Mean standard deviations for $\boldsymbol{RR}$ are 56.6%, 23.4% and 12.7%, and for $\boldsymbol{CEN}$ are 3, 3.4 and 2 weeks. $\boldsymbol{RR}$ variability is notably high in certain basins at northernmost of study domain, likely beyond the true values because of uncertainties in precipitation data (DGA, 2019b; Beck et al., 2019) and numerical issues, as discussed later. $\boldsymbol{LOWV}$ shows no clear spatial patterns, with larger longitudinal variations compared to latitudinal. The standard deviations for the latter variable are 0.09, 0.17 and 0.14 units for snowmelt-driven, mixed and rainfall-driven catchments, respectively.

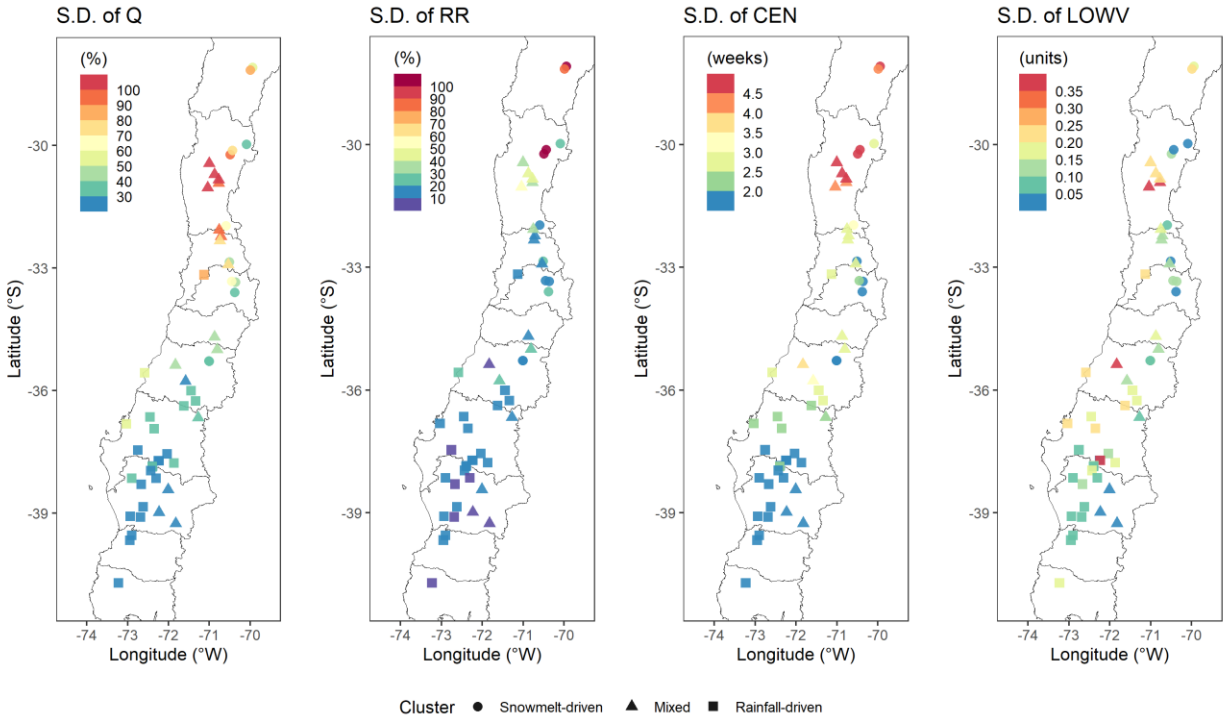


*Figure 3. Standard deviation for annual time series of hydrological signatures. Left to right: streamflow, runoff ratio, centroid of hydrograph, and low-segment volume of the flow duration curve, respectively.*

## 4.2 Connection between ENSO phases and streamflow distributions

As shown in Figure 4, the K-means clustering procedure successfully captures the distinct timing regimes. We compute the confidence intervals (shadowed areas) by nonparametric bootstrapping, in order to avoid the assumption of normality. The rainfall-driven cluster has the narrowest confidence intervals for both precipitation and streamflow, indicating a more homogeneous seasonality compared to snowmelt-driven or mixed regime clusters. We attribute a more heterogeneous seasonality of streamflow to systems with higher regulation capacity. Also, the more heterogeneous distribution of precipitation may indicate spatial features such as orographic precipitation enhancement (due to higher elevations of mixed and snowmelt-driven basins), wider latitudinal distribution of the basins, widespread longitudinal distribution (specially for mixed basins, as shown in Figure 1 and Table 1), and/or another micro-climate conditions.

Figure 4 also displays a stratification based on ENSO-phases, showing similar shapes of El Niño and neutral phases streamflow seasonalities, and a distinct behavior during La Niña years, remarking nonlinearity between ENSO phases. This is, for La Niña (neutral or El Niño) years we notice earlier (later) hydrograph peaks at snowmelt-driven basins, apparent unimodal (bimodal) distribution for mixed catchments, and later (earlier) hydrograph peaks in rainfall-driven watersheds, following the anomalies observed in precipitation distribution.

Since El Niño (La Niña) is related to generally wetter (drier) conditions in the study domain, these anomalies are also reflected on the probability distribution of daily streamflow, as shown by the FDCs in Figure 5. We obtain distinct upper high-segments of FDC during El Niño years in snowmelt-driven and mixed clusters, suggesting major effects of El Niño phases over peak snowmelt rates due to higher accumulation of snowpack (Cortés and Margulis, 2017; Masiokas et al., 2006). However, the opposite relationship – between La Niña and less snowpack – is not well established (Cortés and Margulis, 2017; Masiokas et al., 2006). At the low flow segment of FDCs, all clusters exhibit convergence between El Niño and neutral phases for larger exceedance probabilities. In particular, narrower differences are obtained for the snowmelt-driven cluster (shown at Figure 5-left). We observe the lowest flows during La Niña years, following previously reported connections between meteorological and hydrological droughts, and La Niña episodes (Oertel et al., 2019). The mixed regime cluster shows wider confidence intervals as expected, because of a greater diversity of hydrological processes affecting low-flows.

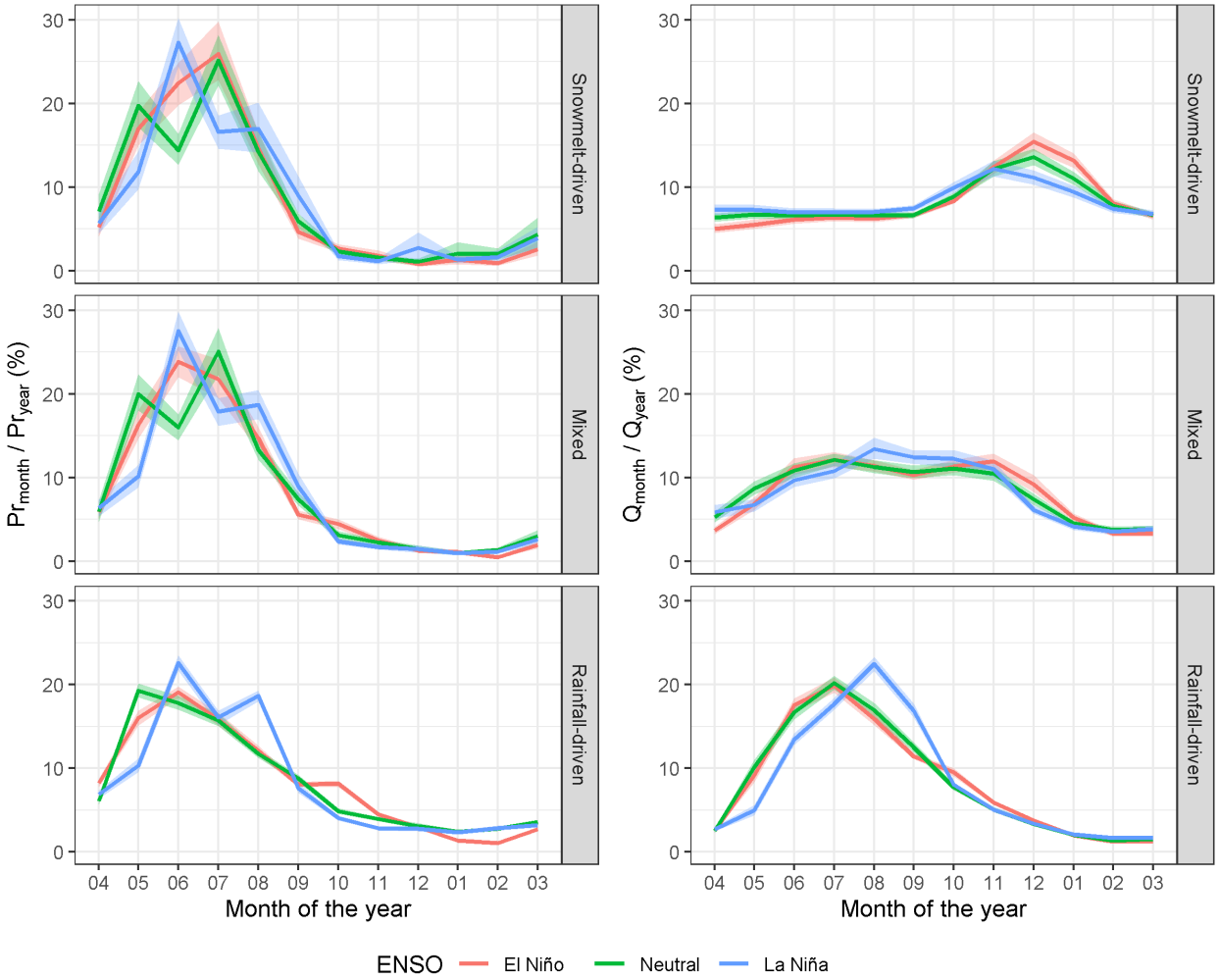


*Figure 4. Seasonality of precipitation (left) and streamflow (right), expressed as fractional coefficients, respectively. Results are stratified by hydrologic regimes and grouped by ENSO type of year. The solid line represents the cluster-averaged values, and the shadowed area indicates 95% confidence intervals obtained with nonparametric bootstrapping.*

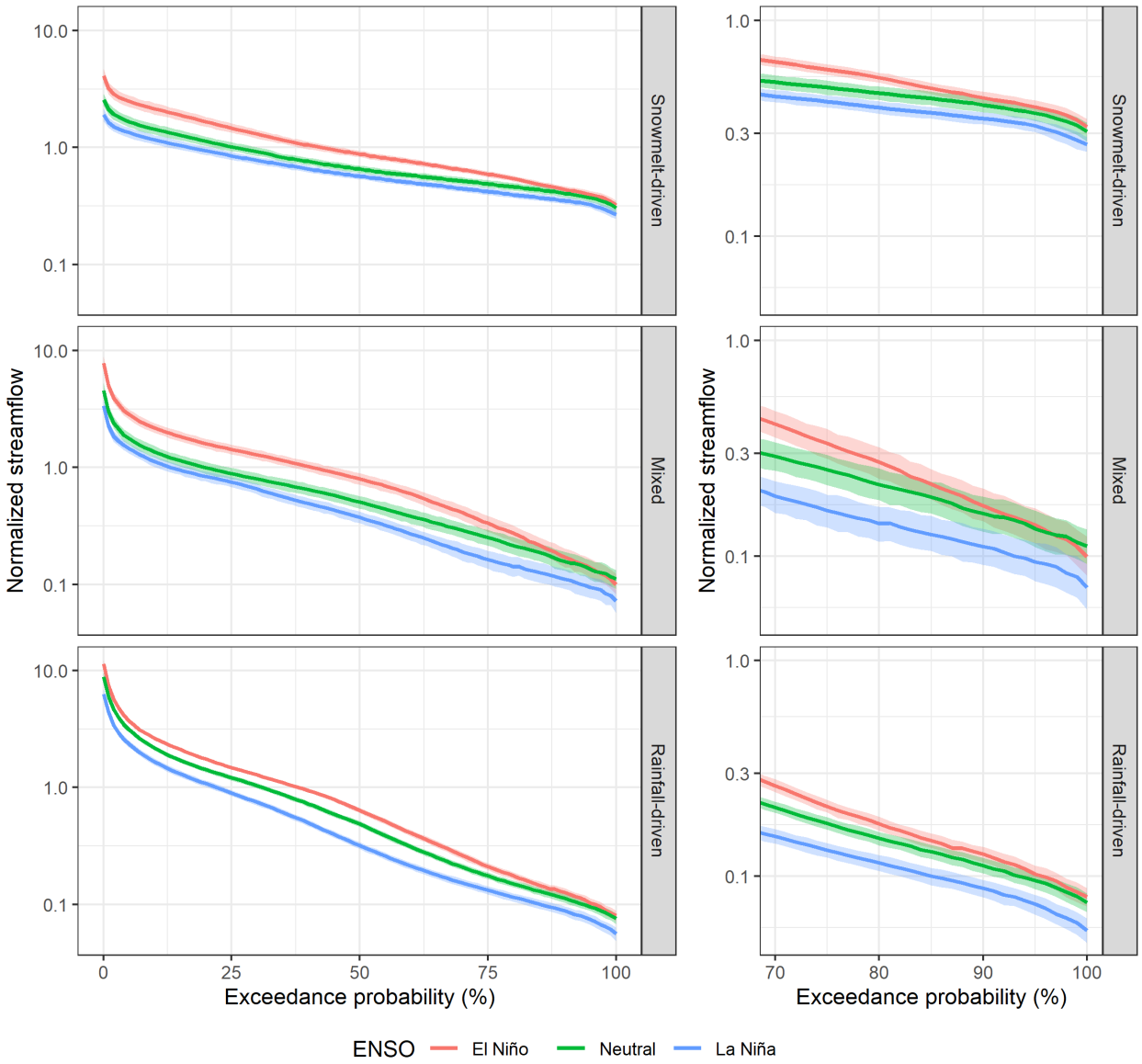


*Figure 5. Flow duration curves of normalized streamflow (left) – daily streamflow over averaged daily streamflow – and zoomed in at the low flow segment of the curve (right). Results are stratified by hydrologic regimes and grouped by ENSO type of year. The solid line represents cluster-averaged values, and the shadowed area indicates the 95% confidence intervals obtained with nonparametric bootstrapping.*

## 4.3 Spatial patterns of composite anomalies

Figure 6 and Figure 7 show composite anomalies – averaged El Niño minus averaged La Niña – for climatic variables and hydrological signatures, respectively. $\boldsymbol{PR_{sto}}$ anomalies are statistically significant for 52 out of 54 basins analyzed, while anomalies of $\boldsymbol{TM_{sto}}$, $\boldsymbol{TM_{win}}$ and $\boldsymbol{TM_{spr}}$ are statistically significant for 37, 39 and 33 basins, respectively, out of 54. Overall, all basins show positive composite anomalies of $\boldsymbol{PR_{sto}}$, $\boldsymbol{TM_{sto}}$ and $\boldsymbol{TM_{win}}$. Composite anomalies for $\boldsymbol{TM_{spr}}$ are negative except for the northern region (below 31 °S). Our results confirm a strong modulation of catchment-scale climatic variables by ENSO in the entire study domain.

We emphasize that $\boldsymbol{PR_{sto}}$ anomalies must be examined in relative terms, since winter precipitation in northern basins is explained just by a few storms, while southern basins have many more days with precipitation during the same season. In this study, a winter storm is detected when a winter day has a cumulative precipitation amount over threshold – 2 mm – at the catchment scale. If we consider storm events with consecutive over-threshold precipitation days during winter, we obtain a mean frequency of 10.5 (19.0) events, and a mean duration of 2.7 (4.8) days, in snowmelt-driven (rainfall-driven) catchments. This is also reflected at the variation coefficients for $\boldsymbol{PR_{sto}}$ of Figure 2.

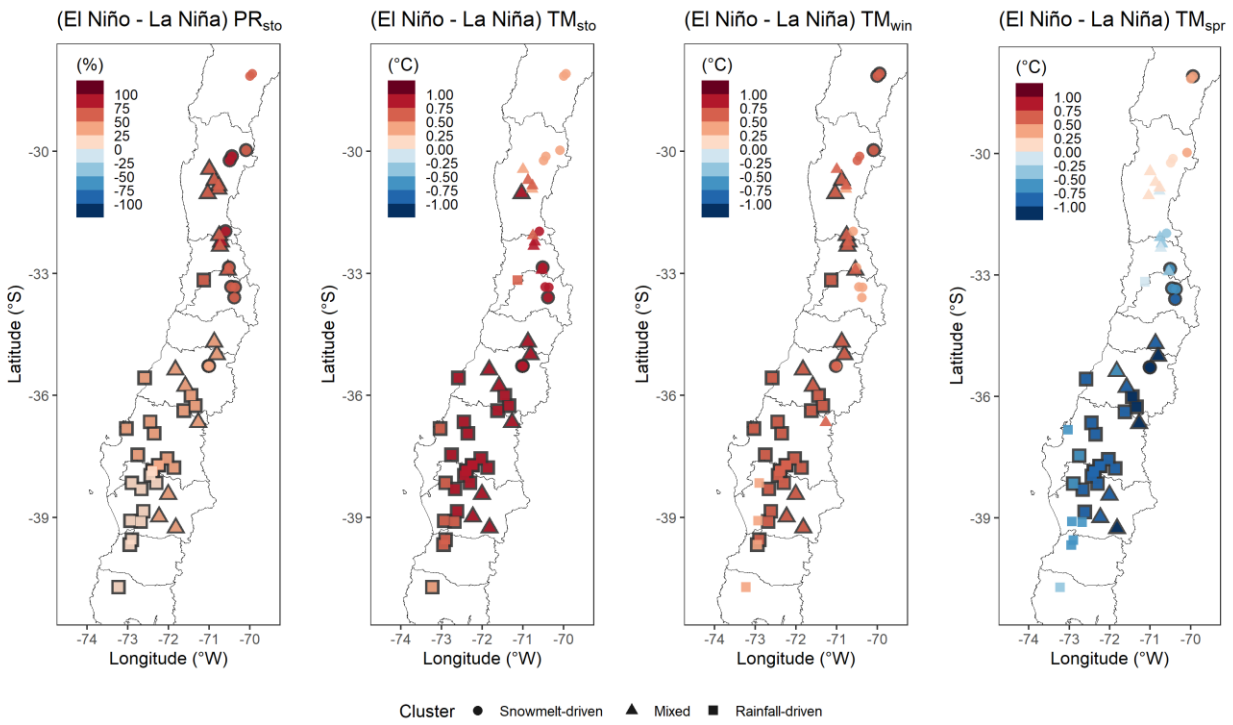


*Figure 6. Composites of El Niño minus composites of La Niña for annual climatic variables. From left to right: precipitation of winter storms, mean temperature of winter storms, mean temperature of winter, and mean temperature of springs, respectively. Stroked markers represent non-zero differences that are statistically significant at the 95% confidence level under the Fisher-Pitman permutation test. The color palette is truncated at the 5% and 95% percentiles for improved visualization.*

Figure 7 shows effects of ENSO on hydrological signatures. For $\boldsymbol{Q}$, composite anomalies are positive across the entire study domain, and differences are statistically significant in almost all basins (50 out of 54). Within-cluster averaging of $\boldsymbol{Q}$ composite (± one standard deviation) results in 56.3 ± 20.3 %, 71.3 ± 33.1 % and 43.3 ± 13.6 %, for snowmelt-driven, mixed and rainfall-driven hydrologic clusters, respectively. These values reflect the strong influence of ENSO on catchment-scale runoff, specially at mixed-regime basins where the anomalies are larger and spatially more heterogenous.

Furthermore, composite anomalies for $\boldsymbol{Q}$ (Figure 7) are greater than those for $\boldsymbol{PR_{sto}}$ (Figure 6) in most cases (43 of 54), except for snowmelt-driven (9 of 12) basins and some mixed-regime basins (2 of 17). The latter match with previous results of $\boldsymbol{Q}$ variability larger than $\boldsymbol{PR_{sto}}$ variability in most of basins (Figure 2 and Figure 3) – since standard deviation and ENSO composites are not a priori supposed to share the same features, it may advise that ENSO is a primary source of variability in the study domain. This nonlinear response – composites of $\boldsymbol{Q}$ greater than composites of $\boldsymbol{PR_{sto}}$ – is consistent with $\boldsymbol{Q}$ elasticity values reported to be larger than 1 by previous studies conducted in other regions of the world (e.g. Sankarasubramanian et al., 2001; Sankarasubramanian and Vogel, 2003; Vano et al., 2012; Berghuijs et al., 2017). Besides nonlinear storage processes, feedback mechanisms may be related with higher water yield efficiency due to favorable antecedent soil moisture. Also, a larger wet day fraction (i.e., fraction of days per year with non-zero precipitation) could be related to local meteorological conditions that reduce the evaporative fraction, through lower atmospheric aridity and cloudier skies. Additionally, Vargas Zeppetello et al. (2019) indicated that a lower (higher) soil moisture content may lead to amplified (softened) sensitivity of surface evaporative cooling to soil moisture variations, attributable to higher (lower) vapor pressure deficits. Because evaporation is mainly controlled by surface temperature, this feedback leads to nonlinear response of evapotranspiration to soil moisture – likewise enhancing the apparent two Budyko regimes (water- and energy-limited environments) and its nonlinearities.

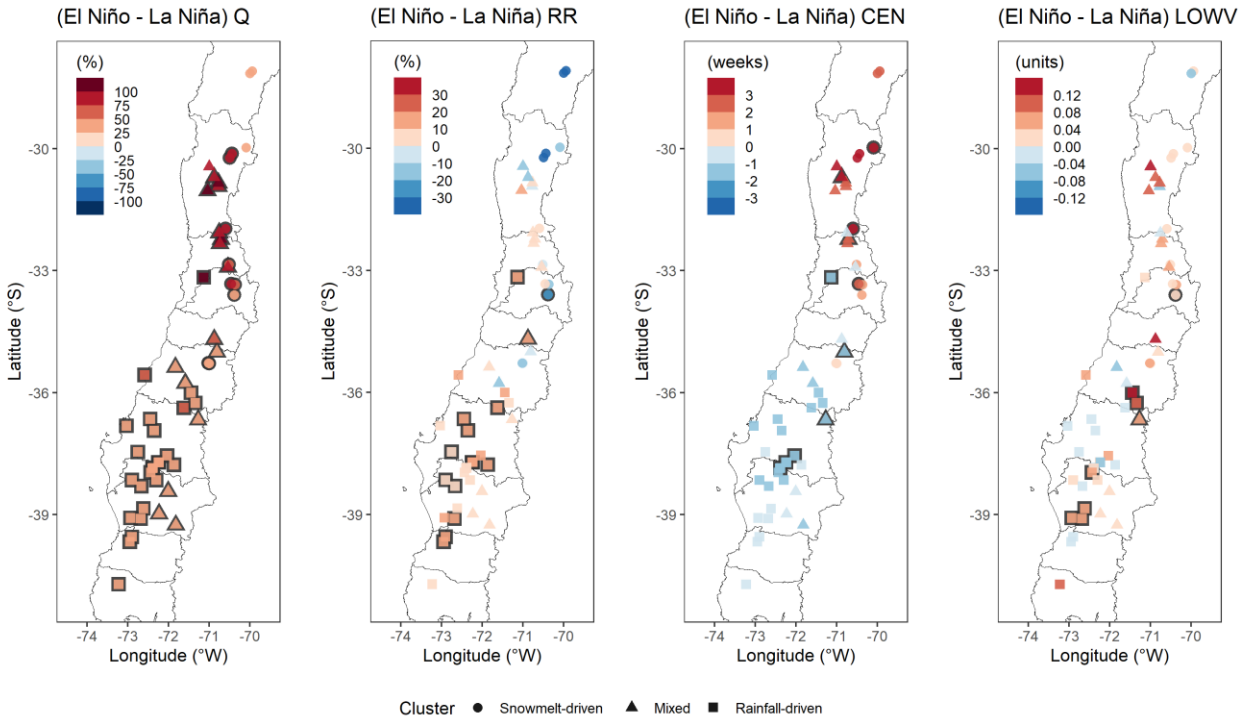


*Figure 7. Composites of El Niño minus composites of La Niña for annual hydrological signatures. From left to right: streamflow, runoff ratio, centroid of hydrograph, and low-segment volume of the flow duration curve, respectively. Stroked markers represent non-zero differences that are statistically significant at the 95% confidence level under the Fisher-Pitman permutation test. The color palette is truncated at the 5% and 95% percentiles for improved visualization.*

As shown in Figure 7, composite anomalies of $\boldsymbol{RR}$ show varied behavior, taking both positive and negative signs across the study domain. Positive composite anomalies are expected because wetter (drier) conditions related to El Niño (La Niña) phase may conduct to higher (lower) water yield efficiency due to favorable (unfavorable) antecedent moisture conditions, also wetter (drier) conditions are related to cloudy (clear) skies such that net radiation may decrease (increase), conducting to lower (higher) actual evapotranspiration. Nevertheless, only for rainfall-driven catchments – humid basins – the cluster-averaged composite anomaly is positive (9.9%), while for mixed regime basins, the averaged composite anomaly is near to zero (0.9%).

Interestingly, cluster-averaged composite anomalies of $\boldsymbol{RR}$ are strongly negative (-20.9%) for snowmelt-driven catchments. Thus, the fraction of water losses may be increased (decreased) during El Niño (La Niña) phase for snowmelt-driven basins. We relate sublimation as a possible reason of water losses behavior. Previous studies using physically-based models at the two-northernmost snowmelt-driven basins of the study domain demonstrate that snow accumulation reaches up to 77% and 87% of total of precipitation on average, and sublimation partition (static evaporation plus dynamic sublimation) arise to 70% and 76% of snow accumulation in mean terms (Jara et al., 2017). Further, composite anomalies of $\boldsymbol{RR}$ are strongly driven by elevation (supplementary Figure B-3). From 3000 m a.s.l. and above, the sublimation partitioning may dominate over the snowmelt partition due to favorable lower temperature during winter and both greater wind speed and solar radiation (Schulz and de Jong, 2004). Accordingly, for basins with mean elevation above 3000 m a.s.l., we obtain negative composite anomalies of $\boldsymbol{RR}$ for almost all basins (8 of 9; all of them snowmelt-driven). The averaged composite anomaly for this subset is -26.1% and the respective standard deviation is 21.4%. For 3500 m a.s.l. as threshold, the values for average and standard deviation are -39.2% and 18.3%, respectively, and all composite anomalies are negatives (5 of 5). However, we note that wind speed variability is not incorporated in our analyses, despite of being a key driver of snow behavior.

$\boldsymbol{CEN}$ shows a clear latitudinal gradient (Figure 7), where hydrologic regimes are enhanced due to ENSO modulation. This pattern is consistent with previous studies (Cortés et al., 2011) and also coherent with results of anomalies in seasonal patterns (Figure 4) and FDCs (Figure 5). For snowmelt-driven basins, $\boldsymbol{CEN}$ composite anomalies are greater than those for the remaining hydrologic regimes (mean 2.2 weeks, i.e., later), associated to larger precipitation anomalies in terms of relative variations (Figure 6). However, for the northernmost region of the domain, composite anomalies of temperature (Figure 6) show higher $\boldsymbol{TM_{sto}}$ – related to fraction of rainfall – and higher $\boldsymbol{TM_{win}}$ – related to snow losses –, which seem to have little effect on $\boldsymbol{CEN}$ anomalies (so on snowpack accumulation) when face against the signal of positive $\boldsymbol{PR_{sto}}$ anomalies. For rainfall-driven catchments, $\boldsymbol{CEN}$ composite anomalies are lower than those for the remaining hydrologic regimes (mean -1.2 weeks, i.e., earlier), while the precipitation distribution within this cluster is lesser winter-concentrated (Figure 4), so the anomalies of $\boldsymbol{PR_{sto}}$ are counterweighted.

Regarding the $\boldsymbol{LOWV}$ – as an alternative proxy to baseflow (McMillan, 2019) –, we find no distinct spatial patterns of ENSO modulation, contrary to composite anomalies of all hydroclimatic variables examined here. In fact, basins with the largest standard deviation (over 50% percentile) of $\boldsymbol{LOWV}$ exhibit averaged composite of ENSO anomalies similar to basins with lowest standard deviation (under 50% percentile), with near to zero difference between both subsets (-0.002 units). The latter suggests that physiographic descriptors (e.g., soil properties, topographic features, geology), in addition to climatic variables, are needed to explain baseflow. However, baseflow process are driven by subsurface and groundwater exchange that may occur on a different or even independent timescale than fast flow (Ghotbi et al., 2020) and the interannual approach of our study does not suffice to provide explanations. Because storage may play a key role on baseflows, Milly et al. (2018) and Milly and Dune (2020) used a simple linear-reservoir correction of streamflow to incorporate year-to-year variations in storage, in the context of improving calculations of streamflow sensitivities to climate. For sake of simplicity, we do not conduct any correction by storage, noting that lag-1 autocorrelation coefficients for annual streamflow are 0.1 ± 0.1 (within-cluster mean ± one standard deviation), 0 ± 0.1 and 0.1 ± 0.1, for snowmelt-driven, mixed and rainfall-driven hydrologic clusters, respectively. The unclear spatial patterns of $\boldsymbol{LOWV}$ reaffirms the importance of physical attributes, besides climatic variables, to explain baseflow behavior.

To better clarify the role of ENSO phases among hydrological clusters, we present anomalies of climatic variables (Figure 8) and hydrological signatures (Figure 9) as boxplots. For snowmelt-driven basins, we obtain averaged anomalies of 35.6%, -36.7% and 68.3% for El Niño, La Niña and difference between both, respectively, for $\boldsymbol{PR_{sto}}$; 30.6%, -25.7% and 56.3% for $\boldsymbol{Q}$; and -9.9%, 11.1% and -20.9% for $\boldsymbol{RR}$. We note that this cluster presents lower $\boldsymbol{RR}$ – interpreted as water yield efficiency – when ENSO conditions are wetter, and vice versa. Further, average anomalies for $\boldsymbol{CEN}$ within this cluster are 1.1 weeks, -1.1 weeks and 2.2 weeks, for El Niño, La Niña and difference between both, respectively (Figure 9-left). Here, we note concomitancy between greater (lower) $\boldsymbol{PR_{sto}}$, later (earlier) $\boldsymbol{CEN}$, and lower (higher) $\boldsymbol{RR}$. Thereby, snowmelt-driven hydrologic catchments seem to attenuate the variability of precipitation over the variability of streamflow accompanied to significant changes in runoff ratio.

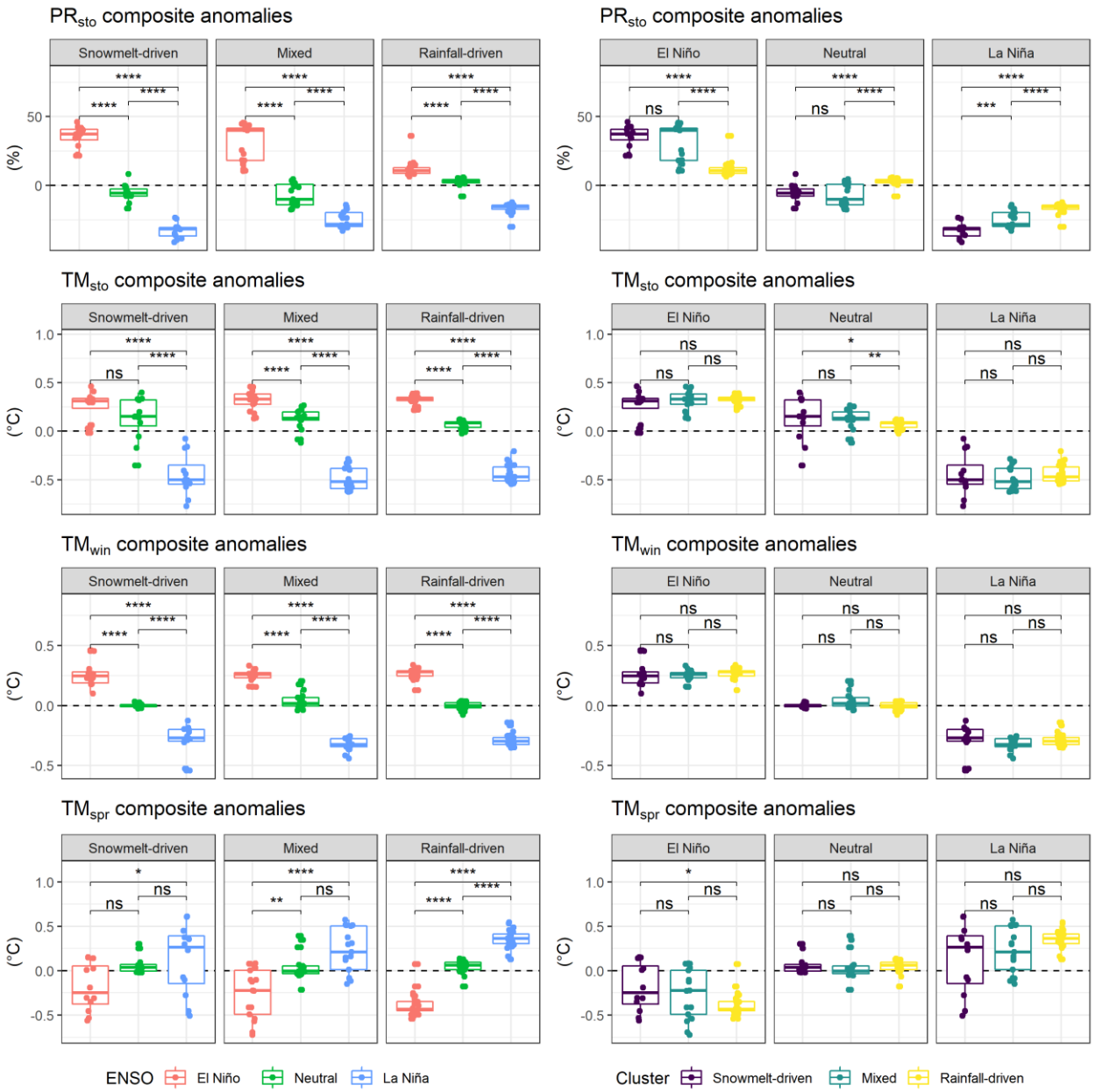


*Figure 8. Composites of ENSO phases for annual climatic variables: precipitation of winter storms, mean temperature of winter storms, mean temperature of winter, and mean temperature of springs, respectively (up to down). Composites are stratified by ENSO type of year (left panel) and by cluster of hydrologic regimes (right panel). Mean differences between groups are assessed under the Wilcoxon test, where ****, ***, **, *, and ns represent statistical significance at the 99.99%, 99.9%, 99%, 95% confidence levels and not significant at the 95% confidence level, respectively.*

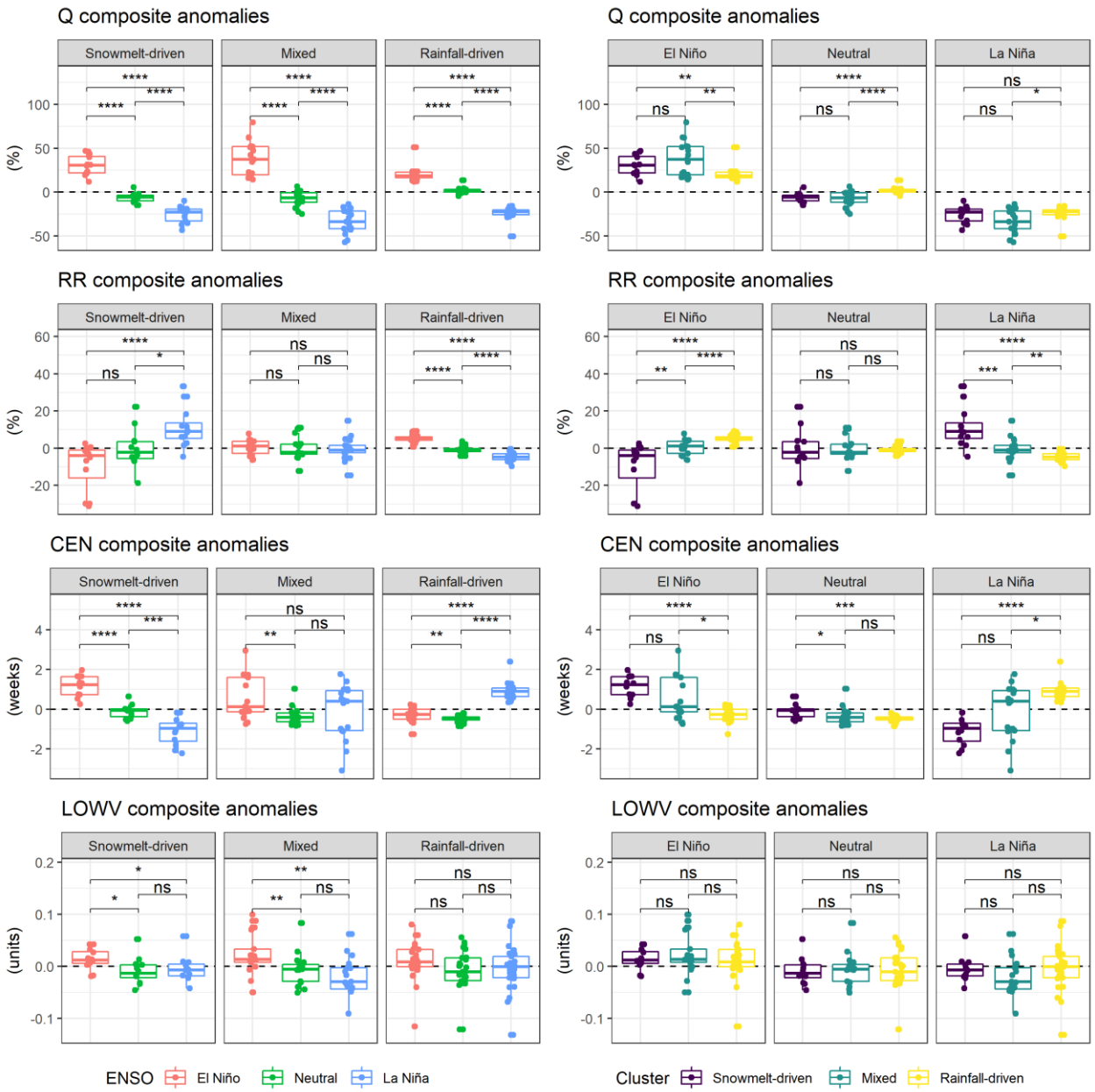


*Figure 9. Composites of ENSO phases for annual hydrological signatures: streamflow, runoff ratio, centroid of hydrograph, and low-segment volume of the flow duration curve, respectively (up to down). Composites are stratified by ENSO type of year (left panel) and by cluster of hydrologic regimes (right panel). Mean differences between groups are assessed under the Wilcoxon test, where ****, ***, **, *, and ns represent statistical significance at the 99.99%, 99.9%, 99%, 95% confidence levels and not significant at the 95% confidence level, respectively.*

From Figure 8 (left) we confirm strong influence of ENSO over the climatic variables – precipitation and temperature – in all hydrologic regimes. When anomalies are grouped by hydrologic regime (Figure 8-right), we note that mostly there are no statistically significant differences between temperature anomalies. Hence, the catchments located within the study domain may be affected by similar $\boldsymbol{TM_{sto}}$, $\boldsymbol{TM_{win}}$ and $\boldsymbol{TM_{spr}}$ variations, due to the ENSO type of year, regardless of their hydrologic regimes. Figure 8 (right) shows a different behavior for $\boldsymbol{PR_{sto}}$, where variations are also modulated by hydrologic regime. The latter is expected because the location of hydrological clusters is confounded with a latitudinal-like hydroclimatic gradient. As shown in Figure 1, snowmelt-driven and rainfall-driven clusters are located in different latitudinal ranges, while variability of $\boldsymbol{PR_{sto}}$ and ENSO modulation in the study domain are driven by latitude, accordingly to Figure 2 and Figure 6, respectively. Additionally, snowmelt-driven and mixed hydrologic regimes enclose catchments with higher average and peak elevations than the rainfall-driven cluster (Table 1), so orographic enhancement of precipitation is a feature already distinguished by clustering classification.

Figure 9 (right) indicates overall no statistically significant differences of ENSO-phases $\boldsymbol{Q}$ anomalies between snowmelt-driven and mixed hydrologic regime clusters, while rainfall-driven catchments show more distinct anomalies due to narrower dispersion. For $\boldsymbol{CEN}$ (Figure 9-right), a similar behavior is observed. $\boldsymbol{RR}$ anomalies are controlled by both ENSO phases and hydrologic regime (Figure 9-left and -right). Differences between averaged $\boldsymbol{RR}$ anomalies of snowmelt-driven and rainfall-driven catchments are quantified as -15%, 0.5% and 15.7% for El Niño, neutral and La Niña, respectively. On the other hand, the differences between within-phase El Niño and La Niña are obtained as -20.9%, 0.9% and 9.9% for snowmelt-driven, mixed and rainfall-driven clusters, respectively, indicating that largest differences in $\boldsymbol{RR}$ are comparable across space (i.e. per basins) and time (i.e. per years). Finally, $\boldsymbol{LOWV}$ show no statistically significant differences when ENSO-phases anomalies are grouped by hydrologic regime (Figure 9-right).

## 4.4 Role of ENSO through hydrologic sensitivities

We examine sensitivities of $\boldsymbol{Q}$ to climatic variables as the total derivative of multiple linear regression models (Figure 10-top). Because sensitivities might lack of historically realistic ranges of variation of climatic variables – precipitation and temperature –, we weight their values by multiplying by composite anomalies of El Niño minus La Niña of Figure 6 (Figure 10-bottom). We prefer to multiply by ENSO composite rather than by standard deviation, because the latter may not be indicative of sign of change during ENSO events.

Sensitivities of $\boldsymbol{Q}$ to $\boldsymbol{PR_{sto}}$ (Figure 10-top) are obtained as (averaged within-cluster ± one standard deviation) 0.77 ± 0.25%%$^{-1}$, 1.09 ± 0.20%%$^{-1}$ and 1.20 ± 0.14%%$^{-1}$, in snowmelt-driven, mixed and rainfall-driven hydrologic regimes, respectively. Overall, sensitivities of streamflow to precipitation are expected to be positive and larger than 1 (e.g. Sankarasubramanian et al., 2001; Sankarasubramanian and Vogel, 2003; Vano et al., 2012; Berghuijs et al., 2017; Milly et al., 2018), with likely higher (smaller) values at arid (humid) environments, due to minor (major) attenuation effects against changes on precipitation. However, sensitivities of streamflow to precipitation are reported to be less than 1 in basins with snowpack storage, related to the role of snowpack on buffering precipitation variability (Sankarasubramanian et al., 2001). Similarly, sensitivities of streamflow to precipitation are reported to be lower and more spatially homogeneous in regions whose temperature and precipitation are in-phase (Sankarasubramanian et al., 2001), where a precipitation surplus is prone to be softened by greater evaporative fraction.

Figure 10 (bottom) displays $\boldsymbol{Q}$ sensitivities multiplied by observed ENSO composite anomalies of $\boldsymbol{PR_{sto}}$ (i.e., weighted sensitivities of $\boldsymbol{Q}$ to $\boldsymbol{PR_{sto}}$), exhibiting greater effects on the northern of the study domain, where ENSO-driven $\boldsymbol{PR_{sto}}$ composite anomalies are larger (Figure 6). For better visualization, we present boxplots of weighted sensitivities of $\boldsymbol{Q}$ in Figure 11. Note that averaged within-cluster weighted $\boldsymbol{Q}$ sensitivities to $\boldsymbol{PR_{sto}}$ (Figure 10-bottom and Figure 11) roughly reach the order of magnitude of ENSO composites of $\boldsymbol{Q}$ (Figure 7), suggesting that $\boldsymbol{Q}$ anomalies during ENSO events are strongly driven by precipitation anomalies rather than temperature anomalies.

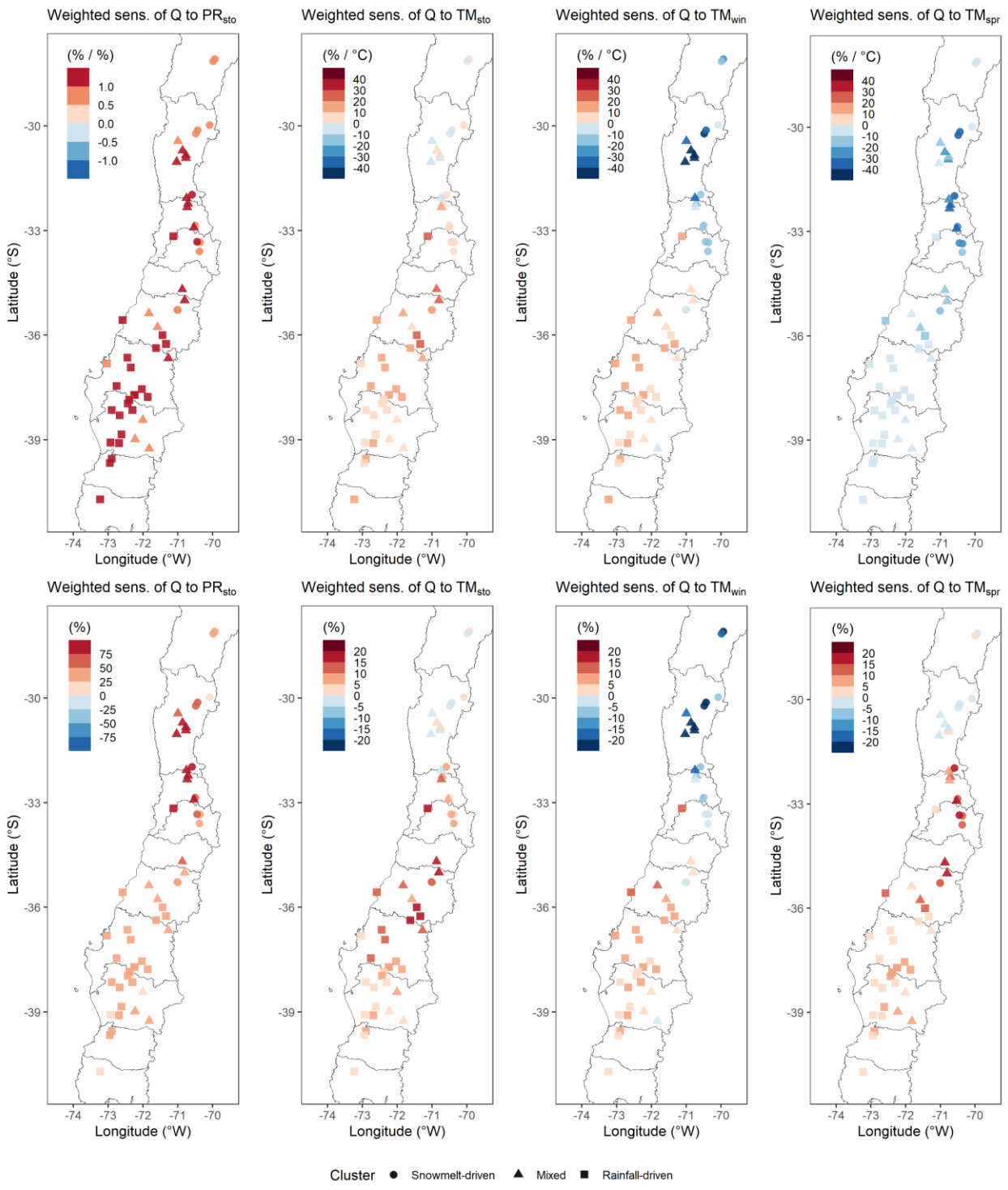


*Figure 10. (Top panel) Left to right: Sensitivities of annual streamflow to winter storm precipitation, winter storm mean temperature, winter mean temperature and spring mean temperature, respectively. (Bottom panel) Same as top but sensitivities are multiplied by El Niño minus La Niña composite anomalies shown at Figure 6. For better visualization, the color palette is truncated at the 5% and 95% percentiles.*

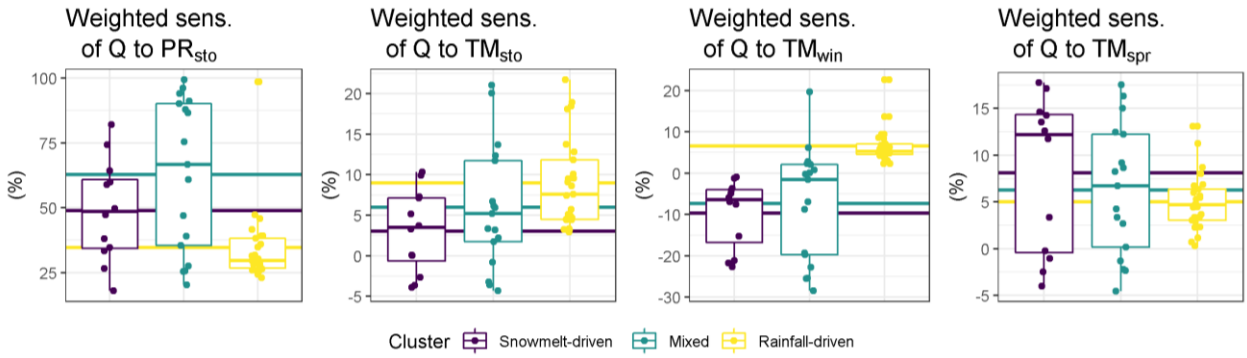


*Figure 11. Boxplots of weighted sensitivities of annual streamflow to winter storm precipitation, mean winter storm temperature, mean winter temperature and mean spring temperature, respectively (left to right). Colored horizontal lines indicate cluster averages. Weighted sensitivities are obtained by multiplying each sensitivity by respective El Niño minus La Niña composite anomalies shown at Figure 6. As a reference, averaged within-cluster ENSO composite anomalies for streamflow are 56.3%, 71.3% and 43.3% in snowmelt-driven, mixed and rainfall-driven hydrologic regimes, respectively (Figure 7).*

We interpret the sensitivities of $\boldsymbol{Q}$ to $\boldsymbol{TM_{sto}}$ (Figure 10-top) as the sensitivity in runoff to changes in the fraction of precipitation falling as rain or snow. This sensitivity is inversely proportional to basin elevation (supplementary Figure B-4). A larger rainfall fraction could be related to favorable antecedent soil moisture for precipitation events during winter, so normalized streamflow would be higher. Also, a smaller snowfall fraction might be related to a general decrease in evaporation and sublimation fluxes, in areas where snowmelt and sublimation dominate. Spatially averaged sensitivities (± one standard deviation) are 2.5 ± 7 %°C$^{-1}$ for snowmelt-driven basins, 6.1 ± 9.1 %°C$^{-1}$ for mixed-regime basins, and 11.7 ± 7.5 %°C$^{-1}$ for rainfall-driven basins. Weighted $\boldsymbol{Q}$ sensitivity to $\boldsymbol{TM_{sto}}$ (Figure 10-bottom) shows that $\boldsymbol{TM_{sto}}$ effects are smaller in northern basins, which are also controlled by snowfall, but it should be noted that the amplitude of ENSO anomalies in this region is smaller (Figure 6). Also, weighted sensitivities (Figure 10-bottom) indicate that the impact of $\boldsymbol{TM_{sto}}$ is also small in southern basins, where elevations (Figure 1) are low enough to make rainfall fraction insensitive to temperature changes.

Despite the attempts to correct multicollinearity effects between explanatory variables on $\boldsymbol{Q}$, this purpose is only partially achieved. In particular, the effects of $\boldsymbol{TM_{sto}}$ and $\boldsymbol{TM_{win}}$ are confounded, especially in rainfall-driven catchments, where a considerably larger number of storms occur. Indeed, the average wet day fraction during winter is 17.4%, 27.8% and 49.3%, in snowmelt-driven, mixed and rainfall-driven catchments, respectively. Nonetheless, Figure 10 (top) shows a clear spatial pattern of $\boldsymbol{Q}$ sensitivities to $\boldsymbol{TM_{win}}$, where northern (southern) and higher (lower) elevation basins tend to have negative (positive) sensitivities. Generally speaking, negative sensitivities of $\boldsymbol{Q}$ to $\boldsymbol{TM_{win}}$ are expected due to an energy surplus that raises the evaporative fraction. Further, negative feedbacks of streamflow to temperature may be invoked due to nonlinear temperature dependence of vapor pressure saturation that affects latent heat fluxes (Milly et al., 2018; Milly & Dunne, 2020). On the other hand, physical processes related to positive sensitivities are commented by Vano et al. (2012) for mid-elevated basins by adopting the "Dettinger hypothesis", which indicates that warmer conditions may produce earlier releasing of water from snowpack storage, at a time of year when evaporative demand is smaller so transformation into runoff is more efficient (e.g., earlier melting of transient snows and/or more liquid fraction of precipitation). Besides, earlier melting of transient snows might induce favorable antecedent moisture conditions for runoff generation during rainfall events. We consider the aforementioned mechanisms as suitable in cold, humid and low-elevated catchments, where positive sensitivities are present (southern of study domain).

We note dissimilar spatial patterns between $\boldsymbol{Q}$ sensitivities against $\boldsymbol{TM_{win}}$ vs. $\boldsymbol{TM_{spr}}$ (Figure 10-top) – both related to snow processes. ENSO composites (Figure 6) show a particular behavior of seasonal temperature anomalies, with warmer (colder) winters during El Niño (La Niña), and cooler (warmer) springs across the study domain, except for northern basins where spring variations are minor and slightly positive (Figure 6). Such peculiar ENSO signal could explain potential shifts in snow processes. Sensitivities of $\boldsymbol{Q}$ to $\boldsymbol{TM_{win}}$ exhibit different signs – negative to northern (high elevation) basins and positive in southern basins –, which may indicate the major effect of snow on climate sensitivities. Accordingly, snow could act as a shield to radiation absorption through albedo, while decreasing albedo in response to rising temperature may dominate the negative sensitivity of streamflow to temperature (Milly and Dunne, 2020). Moreover, snowfall fraction has been positively correlated with streamflow anomalies in time and space (Berghuijs et al., 2014). Similar results with a process-based model were obtained by Milly and Dunne (2020), although distinction between snow albedo and snowfall fraction must be noted as both may be correlated. However, Barnhart et al. (2016) related warming with earlier snowmelt during spring, which may produce slower snowmelt due to less energy available by solar radiation. Thus, earlier and slower snowmelt leads to shallow soil water and decreased baseflow production, moving streamflow to negative anomalies.

Estimated sensitivities of $\boldsymbol{Q}$ to $\boldsymbol{TM_{win}}$ (Figure 10) are -17.1 ± 11.9%°C$^{-1}$, -13.7 ± 23.9%°C$^{-1}$ and 12 ± 7.5%°C$^{-1}$ (averaged within-cluster ± one standard deviation), for snowmelt-driven, mixed and rainfall-driven hydrologic clusters, respectively. In snowmelt-driven and mixed basins, negative sensitivities may be related to reduced albedo, earlier, slower snowmelt, and/or increased latent heat fluxes. Due to noticeable correlation between $\boldsymbol{TM_{sto}}$ and $\boldsymbol{TM_{win}}$ in rainfall-dominated catchments, both sensitivities are similar (11.7 ± 7.5 %°C$^{-1}$ for $\boldsymbol{Q}$ sensitivity to $\boldsymbol{TM_{sto}}$, Figure 10-top), and we relate them to the aforementioned "Dettinger hypothesis". Dichotomous sensitivities signs are also transmitted to weighted sensitivities, as shown at Figure 11.

Overall, we obtain negative sensitivities of $\boldsymbol{Q}$ to $\boldsymbol{TM_{spr}}$ (Figure 10-top), with -17.1 ± 14.2%°C$^{-1}$, -18 ± 12.7%°C$^{-1}$ and -6.5 ± 3.2%°C$^{-1}$, for snowmelt-driven, mixed and rainfall-driven catchments, respectively. For snowmelt-driven and mixed hydrologic clusters, we argue that the same reasoning provided for $\boldsymbol{Q}$ sensitivity to $\boldsymbol{TM_{win}}$ applies. Rainfall-driven basins exhibit smaller $\boldsymbol{Q}$ sensitivity to $\boldsymbol{TM_{spr}}$ (Figure 10-top), presumably due to lack of snow-related feedbacks. However, latent heat fluxes could be enhanced with warming, albeit in this cluster during spring the runoff is slight but still present (Figure 3). Weighted sensitivities of $\boldsymbol{Q}$ to $\boldsymbol{TM_{spr}}$ are smaller in northern basins (Figure 10-bottom), where ENSO effects on spring temperature are small and slightly positive (Figure 6).

Our estimations of streamflow climate sensitivities exhibit coherent patterns, that are consistent with backgrounds. The latter is a primary finding, due to simplicity of estimators as total derivatives of linear models (see Data and methods). Moreover, multiple linear dependences to climate are a priori unrealistic because of nonlinearities of thermodynamics and feedbacks. Streamflow sensitivities to precipitation are within the ranges of previous studies in other regions worldwide, conducted with varied methodologies – empirical nonparametric-based (Sankarasubramanian et al., 2001; Sankarasubramanian and Vogel, 2003), empirical regression-based (Milly et al., 2018), simulation-based (Vano et al., 2012), and Budyko framework-based (Milly et al., 2018). On the other hand, as well as we obtain aforesaid consistent patterns of streamflow sensitivities to temperature, we underpin that these sensitivities are not comparable with those that would be obtained with respect to annual temperature, due to the approach followed here to split temperature time series into storms, winter and spring sub-periods. Besides, lack of simultaneous statistical significance of all regression coefficients related to temperature (see Data and methods) undermines particularly individual values – i.e., per basin. Notwithstanding, we advise that central tendencies might be more trustworthy.

In the context of climate change, historical streamflow sensitivities to climate have been used together with climate projections to obtain streamflow projections in a simple additive scheme (i.e. linear dependent). Further comparisons between physically-based and these empirically-based runoff projections show that historical sensitivities of streamflow to climate are prominent first-order drivers (Lehner et al., 2019). In this work, we carefully adopted this approach by adding weighted sensitivities, obtaining an estimation of streamflow anomalies to roughly assess separate contribution of ENSO climate anomalies to overall ENSO streamflow anomaly. As well as additive principle might be mistrusted due to interactions, Vano et al. (2012) found that added precipitation and temperature changes computed separately are around equal to changes computed combinedly, in physical-based hydrological simulation.

Table 3 shows ENSO $\boldsymbol{Q}$ anomalies estimated by adding weighted sensitivities of $\boldsymbol{Q}$ to climate. Temperature effects are considered in a single term by the sum of all temperature-related weighted sensitivities – i.e., $\boldsymbol{Q}$ to $\boldsymbol{TM_{sto}}$, to $\boldsymbol{TM_{win}}$ and to $\boldsymbol{TM_{spr}}$ (Table 3-[2]). Table 3-[3] is the overall effect of ENSO on $\boldsymbol{Q}$ using the climate sensitivities approach, which is in the order of magnitude than observed ENSO $\boldsymbol{Q}$ composites (Figure 7), as shown in Table 3-[4]. Finally, in order to roughly estimate the effect of ENSO precipitation-anomalies – so ENSO temperature-anomalies, by discarding –, we calculate a ratio (Table 3-[5]) between weighted $\boldsymbol{Q}$ sensitivity to $\boldsymbol{PR_{sto}}$ (Table 3-[1]) and the overall sum of weighted $\boldsymbol{Q}$ climate sensitivities (Table 3-[3]).

Individual basin-related ratios (see Data and methods) are equal or larger than 0.5, suggesting that ENSO-related precipitation variability is the main driver over streamflow variability in all basins across the study domain – in agreement with previous global-scale results (Berghuijs et al., 2017). Besides, central tendencies for these ratios indicate that the effect of ENSO-related $\boldsymbol{PR_{sto}}$ anomalies on ENSO-related $\boldsymbol{Q}$ anomalies is 1.32 ± 0.78 (averaged within-cluster ± one standard deviation) within snowmelt-driven basins. Here, ratio values greater (smaller) than 1 indicate that the temperature effect is counterweighting (compounding) the precipitation aftermath. The ratio values for rainfall-driven and mixed-regime catchments come to 0.63 ± 0.06 and 0.96 ± 0.42, respectively. Thereby, the effects of ENSO-related temperature anomalies in snowmelt-driven (rainfall-driven) catchments may be related to -32% (+37%) – around a third – of compensation (enhancement) of ENSO-related precipitation anomalies effects on $\boldsymbol{Q}$ response. As expected, mixed-regime basins show varied ratio values, reflecting a transition between snowmelt-driven and rainfall-driven outcomes. We emphasize that these precipitation or temperature ratios are highly dispersed among snowmelt-driven and mixed-regime catchments (dispersion is same magnitude order than central value), while for rainfall-driven cluster the dispersion is one order of magnitude lower than the central value.

*Table 3. Estimated ENSO streamflow anomalies by adding weighted sensitivities of streamflow to climate (see in text). *As reference, [4] are observed ENSO composites anomalies of streamflow from Figure 7. By fitting [3] to [4] through linear regression (individual values) we obtain $R^2 = 0.26$ and p-value < 0.0001.*

| Cluster | Snowmelt-driven (averaged within-cluster ± standard deviation) | Mixed (averaged within-cluster ± standard deviation) | Rainfall-driven (averaged within-cluster ± standard deviation) |
|---|---|---|---|
| [1] Weighted sensitivity to precipitation | 48.9 ± 19.6 % | 62.9 ± 29.3 % | 34.6 ± 14.9 % |
| [2] Added weighted sensitivities to temperature | 1.5 ± 20.2 % | 4.9 ± 25.1 % | 20.5 ± 9.4 % |
| [3] Added weighted sensitivities ([1] + [2]) | 50.4 ± 30.2 % | 67.8 ± 26.6 % | 55.1 ± 23.1 % |
| [4] Observed composite* | 56.3 ± 20.3 % | 71.3 ± 33.1 % | 43.6 ± 13.6 % |
| [5] Ratio of precipitation to overall ([1] / [3]) | 1.32 ± 0.78 | 0.96 ± 0.42 | 0.63 ± 0.06 |

A similar climate sensitivity analyses with $\boldsymbol{RR}$ – instead of $\boldsymbol{Q}$ – would be desirable to achieve better understanding of water balance behavior, especially in snow-dominated catchments within the study domain where sublimation may be a key component of evapotranspiration (Jara et al., 2017). We highlight that uncertainties in the true value of precipitation due to undercatch issues across the territory (DGA, 2019b; Beck et al., 2019) may be propagated through annual $\boldsymbol{RR}$. Furthermore, because annual precipitation in northernmost catchments is explained by only a few storms, $\boldsymbol{RR}$ could be undermined by numerical artifacts when precipitation is near to zero. We address the latter as crucial for non-reliable spatial patterns obtained for sensitivities of $\boldsymbol{RR}$ to climate (supplementary Figure B-5).

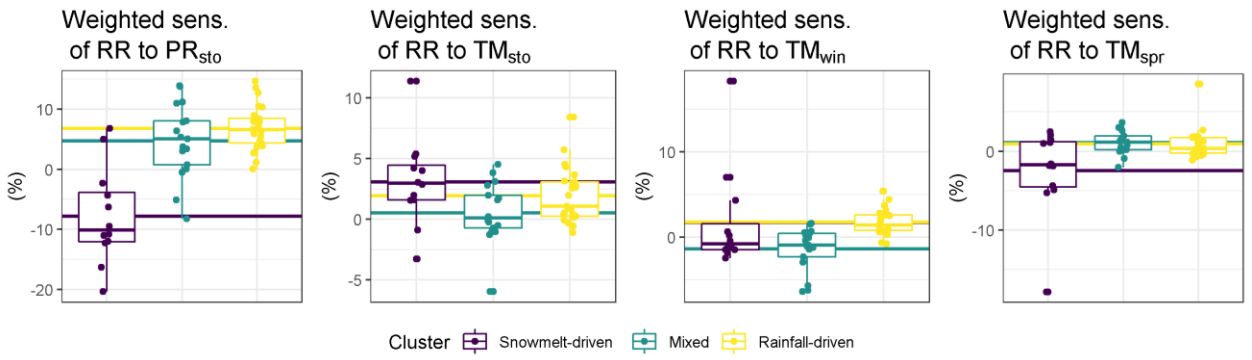


*Figure 12. Boxplots of weighted sensitivities of runoff ratio to winter storm precipitation, mean winter storm temperature, mean winter temperature and mean spring temperature, respectively (left to right). Colored horizontal lines indicate cluster averages. Weighted sensitivities are obtained by multiplying each sensitivity by respective El Niño minus La Niña composite anomalies shown at Figure 6. As a reference, averaged within-cluster ENSO composite anomalies for runoff ratio are -20.9%, 0.9% and 9.9% in snowmelt-driven, mixed and rainfall-driven hydrologic regimes, respectively (Figure 7).*

Figure 12 displays the boxplots of weighted sensitivities of $\boldsymbol{RR}$ to climatic variables. The results indicate that distributions of $\boldsymbol{RR}$ weighted sensitivities are well-centered when grouping by hydrologic cluster. We note that weighted sensitivities of $\boldsymbol{RR}$ to $\boldsymbol{PR_{sto}}$ are prominent in comparison with weighted sensitivities to $\boldsymbol{TM_{sto}}$, $\boldsymbol{TM_{win}}$ and $\boldsymbol{TM_{spr}}$, whose central tendencies are mostly near to zero. In rainfall-driven catchments, we explain positive weighted sensitivities of $\boldsymbol{RR}$ to $\boldsymbol{PR_{sto}}$ by more efficient runoff generation due to antecedent soil moisture conditions. Also, a more humid environment due to ENSO-anomalies of $\boldsymbol{PR_{sto}}$ may enhance the nonlinear response of evapotranspiration processes (e.g. Vargas Zeppetello et al., 2019), affecting $\boldsymbol{RR}$ anomalies. Finally, wetter conditions are related to cloudier skies and less atmospheric aridity, decreasing the evaporative fraction.

On the other hand, the amplitude of cluster-averaged $\boldsymbol{RR}$ composite anomalies in snowmelt-driven basins is larger than for rainfall-driven catchments (-20.9% against 9.9%, respectively; Figure 7 and Figure 9-left), suggesting sharp effects of water losses to atmosphere in snowmelt-driven basins, while rainfall-driven catchments lack of snowmelt- and sublimation-related important losses, showing minor amplitude and a narrower dispersion of individual values – i.e., per basin (Figure 9-left). Thus, for snowmelt-driven basins, since weighted sensitivities of $\boldsymbol{RR}$ to $\boldsymbol{PR_{sto}}$ seem to dominate the overall effect of ENSO on this variable (Figure 12), more (less) precipitation could generate a thicker (shallower) snowpack that remains further (closer) inside the season, being more (less) prone to losses. This relationship enlightens previously reported asymmetries between significantly larger snow accumulation during El Niño, but no notable lack of snowpack during La Niña (Masiokas et al., 2006; Cortés and Margulis, 2017), with remarkable changes in $\boldsymbol{RR}$ through ENSO-phases. Nevertheless, due to beforementioned non-reliable spatial patterns of $\boldsymbol{RR}$ climate sensitivities (supplementary Figure B-5), further analyses for $\boldsymbol{RR}$ are not presented.

Finally, it is worth noting that this work does not analyze ENSO-related variability in several key variables – such as wind, which controls evaporation and snow dynamics by advection of heat and humidity –, physiographic controls – e.g., topography or exposure of catchments to air masses, which may be suggested to relate the patterns of response against ENSO (Mosley, 2000) –, and storm parameters such as duration or frequency, which presumably contribute to nonlinearity of ENSO-related hydrological response (Cayan et al., 1999). Moreover, any perturbation in atmospheric circulation – as ENSO – could perturb the dominant storm patterns, frequency and persistence of precipitation events, which are all related to rainfall-runoff generation mechanisms (Sharma et al., 2018). Nevertheless, this work is aimed to complement other large-sample hydrology studies (Gupta et al., 2014) by unraveling general patterns of ENSO effects on hydroclimatic variables, specifically precipitation, temperature and streamflow signatures. Further understanding of ENSO effects on physical mechanisms, using data from process-based models capable to simulate nonlinear feedbacks, should be contrasted.

# 5 CONCLUSIONS

This work investigates the effects of ENSO-related fluctuations on primary climatic variables – winter precipitation and winter-storms, mean-winter and mean-spring temperatures – and hydrological signatures in Central-Southern Chile. Our results confirm a strong influence of ENSO on catchment-scale climatic variables. Indeed, all catchments across the entire study domain (27°S to 41°S) exhibit statistically significant changes in at least one of the climatic variables analyzed. Due to simultaneous changes in precipitation and temperature, ENSO-related climate effects on the hydrology is not straightforward because of compensatory effects or amplifying signals. Our results show that catchments with different hydrologic regimes provide different catchment responses to ENSO fluctuations, despite the sharper latitudinal and longitudinal controls across the territory that set climate and physiographic characteristics in Central-Southern Chile. The main findings of our work are as follows:

i. ENSO represents a peculiar variability signal along seasonal temperature. At the catchment scale, El Niño (La Niña) events are related to warming (cooling) during winters and cooling (warming) during springs. The latter provides uneven effects over streamflow. We obtain positive sensitivities of streamflow to storm temperature and negative sensitivities to spring temperature in around all basins, but sensitivities of streamflow to mean winter temperature are negative (positive) at northern (southern) catchments within the study domain. This feature is a challenging claim for realistic timing of temperature in water resources estimations, especially for snowy catchments.
ii. In snowmelt-dominated basins, El Niño (La Niña) phase is associated with wetter (drier) conditions and smaller (greater) runoff ratios, as compensatory feedback. Due to large sublimation losses, we presume that this compensatory relationship is driven by precipitation anomalies, where thicker (shallower) snowpack remains for a longer (shorter) time inside the season, being more (less) prone to losses. This relationship reconciles previously observed asymmetries between El Niño and La Niña regarding snow accumulation.
iii. Overall, wetter conditions and warmer (cooler) winters (springs) are observed during El Niño phases compared to La Niña. In snowmelt-driven catchments, temperature anomalies moderate precipitation-induced streamflow responses. Conversely, streamflow anomalies (El Niño minus La Niña) are exacerbated by both precipitation and temperature anomalies in rainfall-driven catchments, compounding 63% and 37%, respectively. These estimates are scattered for snowmelt-driven and mixed regime basins (i.e., dispersion has the same order of magnitude than central tendencies), although the spread is small (i.e., magnitude order below central tendency) in rainfall-driven basins. Therefore, air temperature anomalies play a key role in the integrated streamflow responses to ENSO.
iv. The variability in low-flow volumes (between 100% to 70% exceedance probability) is not primarily controlled by ENSO in the study domain. Moreover, inter-annual variability patterns related to these low-flows do not seem to match with a latitudinal hydroclimatic gradient, suggesting that physical descriptors such as geology and soil properties have a primary role on baseflow generation.

# BIBLIOGRAFÍA


Alvarez-Garreton, C., Mendoza, P. A., Boisier, J. P., Addor, N., Galleguillos, M., Zambrano-Bigiarini, M., ... & Ayala, A. (2018). The CAMELS-CL dataset: catchment attributes and meteorology for large sample studies-Chile dataset. Hydrology and Earth System Sciences, 22(11), 5817-5846.

Barnhart, T. B., Molotch, N. P., Livneh, B., Harpold, A. A., Knowles, J. F., & Schneider, D. (2016). Snowmelt rate dictates streamflow. Geophysical Research Letters, 43(15), 8006-8016.

Beck, H. E., Wood, E. F., McVicar, T. R., Zambrano-Bigiarini, M., Alvarez-Garreton, C., Baez-Villanueva, O. M., ... & Karger, D. N. (2019). Bias correction of global high-resolution precipitation climatologies using streamflow observations from 9372 catchments. Journal of Climate, (2019).

Berghuijs, W. R., Woods, R. A., & Hrachowitz, M. (2014). A precipitation shift from snow towards rain leads to a decrease in streamflow. Nature Climate Change, 4(7), 583.

Berghuijs, W. R., Larsen, J. R., Van Emmerik, T. H., & Woods, R. A. (2017). A global assessment of runoff sensitivity to changes in precipitation, potential evaporation, and other factors. Water Resources Research, 53(10), 8475-8486.

Blöschl, G., Sivapalan, M., Savenije, H., Wagener, T., & Viglione, A. (Eds.). (2013). Runoff prediction in ungauged basins: synthesis across processes, places and scales. Cambridge University Press.

Cayan, D. R., Redmond, K. T., & Riddle, L. G. (1999). ENSO and hydrologic extremes in the western United States. Journal of Climate, 12(9), 2881-2893.

Cortés, G., Vargas, X., & McPhee, J. (2011). Climatic sensitivity of streamflow timing in the extratropical western Andes Cordillera. Journal of Hydrology, 405(1-2), 93-109.

Cortés, G., & Margulis, S. (2017). Impacts of El Niño and La Niña on interannual snow accumulation in the Andes: Results from a high-resolution 31 year reanalysis. Geophysical Research Letters, 44(13), 6859-6867.

Chouaib, W., Caldwell, P. V., & Alila, Y. (2018). Regional variation of flow duration curves in the eastern United States: Process-based analyses of the interaction between climate and landscape properties. Journal of Hydrology, 559, 327-346.

DGA. (2016). Atlas del Agua, Chile 2016. Santiago: Dirección General de Aguas, Ministerio de Obras Públicas. http://www.dga.cl/atlasdelagua/Paginas/default.aspx.

DGA (2019a). Aplicación de la metodología de actualización del Balance Hídrico Nacional en la macrozona sur y parte norte de la macrozona austral, SIT N° 441. Ministerio de Obras Públicas, Dirección General de Aguas, División de Estudios y Planificación, Santiago, Chile. Elaborado por: Universidad de Chile, Facultad de Ciencias Físicas y Matemáticas.

DGA (2019b). Aplicación de la metodología de actualización del Balance Hídrico Nacional en las cuencas de la parte sur de la macrozona austral e Isla de Pascua, SIT N° 444. Ministerio de Obras Públicas, Dirección General de Aguas, División de Estudios y Planificación, Santiago, Chile. Elaborado por: Universidad de Chile, Facultad de Ciencias Físicas y Matemáticas.

Ghotbi, S., Wang, D., Singh, A., Blöschl, G., & Sivapalan, M. (2020). A New Framework for Exploring Process Controls of Flow Duration Curves. Water Resources Research, e2019WR026083.

Grothe, P. R., Cobb, K. M., Liguori, G., Di Lorenzo, E., Capotondi, A., Lu, Y., ... & Deocampo, D. M. (2019). Enhanced El Niño-Southern Oscillation variability in recent decades. *Geophysical Research Letters*.

Gupta, H. V., Perrin, C., Bloschl, G., Montanari, A., Kumar, R., Clark, M., & Andréassian, V. (2014). Large-sample hydrology: a need to balance depth with breadth. Hydrology and Earth System Sciences, 18(2), 463-477.

Hu, S., & Fedorov, A. V. (2016). Exceptionally strong easterly wind burst stalling El Niño of 2014. Proceedings of the National Academy of Sciences, 113(8), 2005-2010.

Jara, F., McPhee, J., Lagos-Zúñiga, M., & Fuster, R. (2017). Sublimación nival en la Cuenca alta del Río Copiapó. In: XXIII Congreso Chileno de Ingeniería Hidráulica. Valparaíso, Chile.

Josse, J., & Husson, F. (2016). missMDA: a package for handling missing values in multivariate data analysis. Journal of Statistical Software, 70(1), 1-31.

Lehner, F., Wood, A. W., Vano, J. A., Lawrence, D. M., Clark, M. P., & Mankin, J. S. (2019). The potential to reduce uncertainty in regional runoff projections from climate models. Nature Climate Change, 9(12), 926-933.

Masiokas, M. H., Villalba, R., Luckman, B. H., Le Quesne, C., & Aravena, J. C. (2006). Snowpack variations in the central Andes of Argentina and Chile, 1951–2005: Large-scale atmospheric influences and implications for water resources in the region. Journal of Climate, 19(24), 6334-6352.

McMillan, H., Westerberg, I., & Branger, F. (2017). Five guidelines for selecting hydrological signatures. Hydrological Processes, 31 (26), 4757-4761.

McMillan, H. (2019). Linking hydrologic signatures to hydrologic processes: A Review. Hydrological Processes.

Milly, P. C. D., & Dunne, K. A. (2020). Colorado River flow dwindles as warming-driven loss of reflective snow energizes evaporation. Science.

Milly, P. C., Kam, J., & Dunne, K. A. (2018). On the sensitivity of annual streamflow to air temperature. Water Resources Research, 54(4), 2624-2641.

Min, Q., Su, J., Zhang, R., & Rong, X. (2015). What hindered the El Niño pattern in 2014?. Geophysical Research Letters, 42(16), 6762-6770.

Montecinos, A., & Aceituno, P. (2003). Seasonality of the ENSO-related rainfall variability in central Chile and associated circulation anomalies. *Journal of Climate*, *16*(2), 281-296.

Mosley, M. P. (2000). Regional differences in the effects of El Niño and La Niña on low flows and floods. Hydrological Sciences Journal, 45(2), 249-267.

Oertel, M., Meza, F. J., & Gironás, J. (2019). Observed trends and relationships between ENSO and standardized hydrometeorological drought indices in central Chile. Hydrological Processes.

Rubio-Álvarez, E., & McPhee, J. (2010). Patterns of spatial and temporal variability in streamflow records in south central Chile in the period 1952–2003. Water Resources Research, 46(5).

Sankarasubramanian, A., Vogel, R. M., & Limbrunner, J. F. (2001). Climate elasticity of streamflow in the United States. Water Resources Research, 37(6), 1771-1781.

Sankarasubramanian, A., & Vogel, R. M. (2003). Hydroclimatology of the continental United States. Geophysical Research Letters, 30(7).

Schulz, O., & de Jong, C. (2004). Snowmelt and sublimation: field experiments and modelling in the High Atlas Mountains of Morocco. Hydrology and Earth System Sciences Discussions, 8(6), 1076-1089.

Sharma, A., Wasko, C., & Lettenmaier, D. P. (2018). If precipitation extremes are increasing, why aren't floods?. *Water Resources Research*, *54*(11), 8545-8551.

Timmermann, A., An, S. I., Kug, J. S., Jin, F. F., Cai, W., Capotondi, A., ... & Stein, K. (2018). El Niño–southern oscillation complexity. Nature, 559(7715), 535-545.

Vano, J. A., Das, T., & Lettenmaier, D. P. (2012). Hydrologic sensitivities of Colorado River runoff to changes in precipitation and temperature. Journal of Hydrometeorology, 13(3), 932-949.

Vargas Zeppetello, L. R., Battisti, D. S., & Baker, M. B. (2019). The Origin of Soil Moisture Evaporation “Regimes”. Journal of Climate, 32(20), 6939-6960.

Viale, M., Valenzuela, R., Garreaud, R. D., & Ralph, F. M. (2018). Impacts of atmospheric rivers on precipitation in southern South America. *Journal of Hydrometeorology*, *19*(10), 1671-1687.

Waylen, P. R., Caviedes, C. N., & Juricic, C. (1993). El Niño-Southern Oscillation and the surface hydrology of Chile: a window on the future?. *Canadian Water Resources Journal*, *18*(4), 425-441.

Wolter, K., & Timlin, M. S. (2011). El Niño/Southern Oscillation behaviour since 1871 as diagnosed in an extended multivariate ENSO index (MEI.ext). International Journal of Climatology, 31(7), 1074-1087.

Yaeger, M., Coopersmith, E., Ye, S., Cheng, L., Viglione, A., & Sivapalan, M. (2012). Exploring the physical controls of regional patterns of flow duration curves–Part 4: A synthesis of empirical analysis, process modeling and catchment classification. Hydrology and Earth System Sciences, 16(11), 4483-4498.

Yilmaz, K. K., Gupta, H. V., & Wagener, T. (2008). A process-based diagnostic approach to model evaluation: Application to the NWS distributed hydrologic model. Water Resources Research, 44(9).

Yokoo, Y., & Sivapalan, M. (2011). Towards reconstruction of the flow duration curve: development of a conceptual framework with a physical basis. Hydrology and Earth System Sciences, 15(9), 2805-2819.

Yu, J. Y., & Kim, S. T. (2013). Identifying the types of major El Niño events since 1870. International Journal of Climatology, 33(8), 2105-2112.

Zheng, F., & Yu, J. Y. (2017). Contrasting the skills and biases of deterministic predictions for the two types of El Niño. Advances in Atmospheric Sciences, 34(12), 1395-1403.

# ANEXO Y APÉNDICES

Se presentan dos anexos con los siguientes contenidos:

1. Material Suplementario A. Ecuaciones explícitas (sistemas 4x4) para cada una de las siguientes sensibilidades:
   - Sensibilidad de $\boldsymbol{Q}$ a $\boldsymbol{PR_{sto}}$
   - Sensibilidad de $\boldsymbol{Q}$ a $\boldsymbol{TM_{sto}}$
   - Sensibilidad de $\boldsymbol{Q}$ a $\boldsymbol{TM_{win}}$
   - Sensibilidad de $\boldsymbol{Q}$ a $\boldsymbol{TM_{spr}}$
   - Sensibilidad de $\boldsymbol{RR}$ a $\boldsymbol{PR_{sto}}$
   - Sensibilidad de $\boldsymbol{RR}$ a $\boldsymbol{TM_{sto}}$
   - Sensibilidad de $\boldsymbol{RR}$ a $\boldsymbol{TM_{win}}$
   - Sensibilidad de $\boldsymbol{RR}$ a $\boldsymbol{TM_{spr}}$

2. Material Suplementario B. Resultados no presentados en texto principal:
   - Curvas estacionales de cuencas, comparadas con los resultados del procedimiento de clasificación de regímenes hidrológicos.
   - Clasificación de años según fases ENSO.
   - Estadísticos resumen (F-test y t-test) de modelos de regresión lineal múltiple.
   - Control altitudinal de anomalías de coeficiente de escorrentía.
   - Control altitudinal de sensibilidades de caudal anual según temperatura media de tormentas de invierno.
   - Patrones espaciales de sensibilidades climáticas del coeficiente de escorrentía.

# SUPPLEMENTARY A

- Equations system (4x4) for sensitivity of $\boldsymbol{Q}$ to $\boldsymbol{PR_{sto}}$. The total derivatives are the unknowns and the partial derivatives are approximated as regression coefficients by least-squares:

$$Sensitivity\ of\ \boldsymbol{Q}\ to\ \boldsymbol{PR_{sto}} := \frac{dQ}{dPR_{sto}}$$

$$\frac{dQ}{dPR_{sto}} = \frac{\partial Q}{\partial PR_{sto}} + \frac{\partial Q}{\partial TM_{sto}} \cdot \frac{dTM_{sto}}{dPR_{sto}} + \frac{\partial Q}{\partial TM_{win}} \cdot \frac{dTM_{win}}{dPR_{sto}} + \frac{\partial Q}{\partial TM_{spr}} \cdot \frac{dTM_{spr}}{dPR_{sto}}$$

$$\frac{dTM_{sto}}{dPR_{sto}} = \frac{\partial TM_{sto}}{\partial PR_{sto}} + \frac{\partial TM_{sto}}{\partial TM_{win}} \cdot \frac{dTM_{win}}{dPR_{sto}} + \frac{\partial TM_{sto}}{\partial TM_{spr}} \cdot \frac{dTM_{spr}}{dPR_{sto}}$$

$$\frac{dTM_{win}}{dPR_{sto}} = \frac{\partial TM_{win}}{\partial PR_{sto}} + \frac{\partial TM_{win}}{\partial TM_{sto}} \cdot \frac{dTM_{sto}}{dPR_{sto}} + \frac{\partial TM_{win}}{\partial TM_{spr}} \cdot \frac{dTM_{spr}}{dPR_{sto}}$$

$$\frac{dTM_{spr}}{dPR_{sto}} = \frac{\partial TM_{spr}}{\partial PR_{sto}} + \frac{\partial TM_{spr}}{\partial TM_{sto}} \cdot \frac{dTM_{sto}}{dPR_{sto}} + \frac{\partial TM_{spr}}{\partial TM_{win}} \cdot \frac{dTM_{win}}{dPR_{sto}}$$

- Equations system (4x4) for sensitivity of $\boldsymbol{Q}$ to $\boldsymbol{TM_{sto}}$. The total derivatives are the unknowns and the partial derivatives are approximated as regression coefficients by least-squares:

$$Sensitivity\ of\ \boldsymbol{Q}\ to\ \boldsymbol{TM_{sto}} := \frac{dQ}{dTM_{sto}}$$

$$\frac{dQ}{dTM_{sto}} = \frac{\partial Q}{\partial TM_{sto}} + \frac{\partial Q}{\partial PR_{sto}} \cdot \frac{dPR_{sto}}{dTM_{sto}} + \frac{\partial Q}{\partial TM_{win}} \cdot \frac{dTM_{win}}{dTM_{sto}} + \frac{\partial Q}{\partial TM_{spr}} \cdot \frac{dTM_{spr}}{dTM_{sto}}$$

$$\frac{dPR_{sto}}{dTM_{sto}} = \frac{\partial PR_{sto}}{\partial TM_{sto}} + \frac{\partial PR_{sto}}{\partial TM_{win}} \cdot \frac{dTM_{win}}{dTM_{sto}} + \frac{\partial PR_{sto}}{\partial TM_{spr}} \cdot \frac{dTM_{spr}}{dTM_{sto}}$$

$$\frac{dTM_{win}}{dTM_{sto}} = \frac{\partial TM_{win}}{\partial TM_{sto}} + \frac{\partial TM_{win}}{\partial PR_{sto}} \cdot \frac{dPR_{sto}}{dTM_{sto}} + \frac{\partial TM_{win}}{\partial TM_{spr}} \cdot \frac{dTM_{spr}}{dTM_{sto}}$$

$$\frac{dTM_{spr}}{dTM_{sto}} = \frac{\partial TM_{spr}}{\partial TM_{sto}} + \frac{\partial TM_{spr}}{\partial PR_{sto}} \cdot \frac{dPR_{sto}}{dTM_{sto}} + \frac{\partial TM_{spr}}{\partial TM_{win}} \cdot \frac{dTM_{win}}{dTM_{sto}}$$

- Equations system (4x4) for sensitivity of $\boldsymbol{Q}$ to $\boldsymbol{TM_{win}}$. The total derivatives are the unknowns and the partial derivatives are approximated as regression coefficients by least-squares:

$$Sensitivity\ of\ \boldsymbol{Q}\ to\ \boldsymbol{TM_{win}} := \frac{dQ}{dTM_{win}}$$

$$\frac{dQ}{dTM_{win}} = \frac{\partial Q}{\partial TM_{win}} + \frac{\partial Q}{\partial PR_{sto}} \cdot \frac{dPR_{sto}}{dTM_{win}} + \frac{\partial Q}{\partial TM_{sto}} \cdot \frac{dTM_{sto}}{dTM_{win}} + \frac{\partial Q}{\partial TM_{spr}} \cdot \frac{dTM_{spr}}{dTM_{win}}$$

$$\frac{dPR_{sto}}{dTM_{win}} = \frac{\partial PR_{sto}}{\partial TM_{win}} + \frac{\partial PR_{sto}}{\partial TM_{sto}} \cdot \frac{dTM_{sto}}{dTM_{win}} + \frac{\partial PR_{sto}}{\partial TM_{spr}} \cdot \frac{dTM_{spr}}{dTM_{win}}$$

$$\frac{dTM_{sto}}{dTM_{win}} = \frac{\partial TM_{sto}}{\partial TM_{win}} + \frac{\partial TM_{sto}}{\partial PR_{sto}} \cdot \frac{dPR_{sto}}{dTM_{win}} + \frac{\partial TM_{sto}}{\partial TM_{spr}} \cdot \frac{dTM_{spr}}{dTM_{win}}$$

$$\frac{dTM_{spr}}{dTM_{win}} = \frac{\partial TM_{spr}}{\partial TM_{win}} + \frac{\partial TM_{spr}}{\partial PR_{sto}} \cdot \frac{dPR_{sto}}{dTM_{win}} + \frac{\partial TM_{spr}}{\partial TM_{sto}} \cdot \frac{dTM_{sto}}{dTM_{win}}$$

- Equations system (4x4) for sensitivity of $\boldsymbol{Q}$ to $\boldsymbol{TM_{spr}}$. The total derivatives are the unknowns and the partial derivatives are approximated as regression coefficients by least-squares:

$$Sensitivity\ of\ \boldsymbol{Q}\ to\ \boldsymbol{TM_{spr}} := \frac{dQ}{dTM_{spr}}$$

$$\frac{dQ}{dTM_{spr}} = \frac{\partial Q}{\partial TM_{spr}} + \frac{\partial Q}{\partial PR_{sto}} \cdot \frac{dPR_{sto}}{dTM_{spr}} + \frac{\partial Q}{\partial TM_{sto}} \cdot \frac{dTM_{sto}}{dTM_{spr}} + \frac{\partial Q}{\partial TM_{win}} \cdot \frac{dTM_{win}}{dTM_{spr}}$$

$$\frac{dPR_{sto}}{dTM_{spr}} = \frac{\partial PR_{sto}}{\partial TM_{spr}} + \frac{\partial PR_{sto}}{\partial TM_{sto}} \cdot \frac{dTM_{sto}}{dTM_{spr}} + \frac{\partial PR_{sto}}{\partial TM_{win}} \cdot \frac{dTM_{win}}{dTM_{spr}}$$

$$\frac{dTM_{sto}}{dTM_{spr}} = \frac{\partial TM_{sto}}{\partial TM_{spr}} + \frac{\partial TM_{sto}}{\partial PR_{sto}} \cdot \frac{dPR_{sto}}{dTM_{spr}} + \frac{\partial TM_{sto}}{\partial TM_{win}} \cdot \frac{dTM_{win}}{dTM_{spr}}$$

$$\frac{dTM_{win}}{dTM_{spr}} = \frac{\partial TM_{win}}{\partial TM_{spr}} + \frac{\partial TM_{win}}{\partial PR_{sto}} \cdot \frac{dPR_{sto}}{dTM_{spr}} + \frac{\partial TM_{win}}{\partial TM_{sto}} \cdot \frac{dTM_{sto}}{dTM_{spr}}$$

- Equations system (4x4) for sensitivity of $\boldsymbol{RR}$ to $\boldsymbol{PR_{sto}}$. The total derivatives are the unknowns and the partial derivatives are approximated as regression coefficients by least-squares:

$$Sensitivity\ of\ \boldsymbol{RR}\ to\ \boldsymbol{PR_{sto}} := \frac{dRR}{dPR_{sto}}$$

$$\frac{dRR}{dPR_{sto}} = \frac{\partial RR}{\partial PR_{sto}} + \frac{\partial RR}{\partial TM_{sto}} \cdot \frac{dTM_{sto}}{dPR_{sto}} + \frac{\partial RR}{\partial TM_{win}} \cdot \frac{dTM_{win}}{dPR_{sto}} + \frac{\partial RR}{\partial TM_{spr}} \cdot \frac{dTM_{spr}}{dPR_{sto}}$$

$$\frac{dTM_{sto}}{dPR_{sto}} = \frac{\partial TM_{sto}}{\partial PR_{sto}} + \frac{\partial TM_{sto}}{\partial TM_{win}} \cdot \frac{dTM_{win}}{dPR_{sto}} + \frac{\partial TM_{sto}}{\partial TM_{spr}} \cdot \frac{dTM_{spr}}{dPR_{sto}}$$

$$\frac{dTM_{win}}{dPR_{sto}} = \frac{\partial TM_{win}}{\partial PR_{sto}} + \frac{\partial TM_{win}}{\partial TM_{sto}} \cdot \frac{dTM_{sto}}{dPR_{sto}} + \frac{\partial TM_{win}}{\partial TM_{spr}} \cdot \frac{dTM_{spr}}{dPR_{sto}}$$

$$\frac{dTM_{spr}}{dPR_{sto}} = \frac{\partial TM_{spr}}{\partial PR_{sto}} + \frac{\partial TM_{spr}}{\partial TM_{sto}} \cdot \frac{dTM_{sto}}{dPR_{sto}} + \frac{\partial TM_{spr}}{\partial TM_{win}} \cdot \frac{dTM_{win}}{dPR_{sto}}$$

- Equations system (4x4) for sensitivity of $\boldsymbol{RR}$ to $\boldsymbol{TM_{sto}}$. The total derivatives are the unknowns and the partial derivatives are approximated as regression coefficients by least-squares:

$$Sensitivity\ of\ \boldsymbol{RR}\ to\ \boldsymbol{TM_{sto}} := \frac{dRR}{dTM_{sto}}$$

$$\frac{dRR}{dTM_{sto}} = \frac{\partial RR}{\partial TM_{sto}} + \frac{\partial RR}{\partial PR_{sto}} \cdot \frac{dPR_{sto}}{dTM_{sto}} + \frac{\partial RR}{\partial TM_{win}} \cdot \frac{dTM_{win}}{dTM_{sto}} + \frac{\partial RR}{\partial TM_{spr}} \cdot \frac{dTM_{spr}}{dTM_{sto}}$$

$$\frac{dPR_{sto}}{dTM_{sto}} = \frac{\partial PR_{sto}}{\partial TM_{sto}} + \frac{\partial PR_{sto}}{\partial TM_{win}} \cdot \frac{dTM_{win}}{dTM_{sto}} + \frac{\partial PR_{sto}}{\partial TM_{spr}} \cdot \frac{dTM_{spr}}{dTM_{sto}}$$

$$\frac{dTM_{win}}{dTM_{sto}} = \frac{\partial TM_{win}}{\partial TM_{sto}} + \frac{\partial TM_{win}}{\partial PR_{sto}} \cdot \frac{dPR_{sto}}{dTM_{sto}} + \frac{\partial TM_{win}}{\partial TM_{spr}} \cdot \frac{dTM_{spr}}{dTM_{sto}}$$

$$\frac{dTM_{spr}}{dTM_{sto}} = \frac{\partial TM_{spr}}{\partial TM_{sto}} + \frac{\partial TM_{spr}}{\partial PR_{sto}} \cdot \frac{dPR_{sto}}{dTM_{sto}} + \frac{\partial TM_{spr}}{\partial TM_{win}} \cdot \frac{dTM_{win}}{dTM_{sto}}$$

- Equations system (4x4) for sensitivity of $\boldsymbol{RR}$ to $\boldsymbol{TM_{win}}$. The total derivatives are the unknowns and the partial derivatives are approximated as regression coefficients by least-squares:

$$Sensitivity\ of\ \boldsymbol{RR}\ to\ \boldsymbol{TM_{win}} := \frac{dRR}{dTM_{win}}$$

$$\frac{dRR}{dTM_{win}} = \frac{\partial RR}{\partial TM_{win}} + \frac{\partial RR}{\partial PR_{sto}} \cdot \frac{dPR_{sto}}{dTM_{win}} + \frac{\partial RR}{\partial TM_{sto}} \cdot \frac{dTM_{sto}}{dTM_{win}} + \frac{\partial RR}{\partial TM_{spr}} \cdot \frac{dTM_{spr}}{dTM_{win}}$$

$$\frac{dPR_{sto}}{dTM_{win}} = \frac{\partial PR_{sto}}{\partial TM_{win}} + \frac{\partial PR_{sto}}{\partial TM_{sto}} \cdot \frac{dTM_{sto}}{dTM_{win}} + \frac{\partial PR_{sto}}{\partial TM_{spr}} \cdot \frac{dTM_{spr}}{dTM_{win}}$$

$$\frac{dTM_{sto}}{dTM_{win}} = \frac{\partial TM_{sto}}{\partial TM_{win}} + \frac{\partial TM_{sto}}{\partial PR_{sto}} \cdot \frac{dPR_{sto}}{dTM_{win}} + \frac{\partial TM_{sto}}{\partial TM_{spr}} \cdot \frac{dTM_{spr}}{dTM_{win}}$$

$$\frac{dTM_{spr}}{dTM_{win}} = \frac{\partial TM_{spr}}{\partial TM_{win}} + \frac{\partial TM_{spr}}{\partial PR_{sto}} \cdot \frac{dPR_{sto}}{dTM_{win}} + \frac{\partial TM_{spr}}{\partial TM_{sto}} \cdot \frac{dTM_{sto}}{dTM_{win}}$$

- Equations system (4x4) for sensitivity of $\boldsymbol{RR}$ to $\boldsymbol{TM_{spr}}$. The total derivatives are the unknowns and the partial derivatives are approximated as regression coefficients by least-squares:

$$Sensitivity\ of\ \boldsymbol{RR}\ to\ \boldsymbol{TM_{spr}} := \frac{dRR}{dTM_{spr}}$$

$$\frac{dRR}{dTM_{spr}} = \frac{\partial RR}{\partial TM_{spr}} + \frac{\partial RR}{\partial PR_{sto}} \cdot \frac{dPR_{sto}}{dTM_{spr}} + \frac{\partial RR}{\partial TM_{sto}} \cdot \frac{dTM_{sto}}{dTM_{spr}} + \frac{\partial RR}{\partial TM_{win}} \cdot \frac{dTM_{win}}{dTM_{spr}}$$

$$\frac{dPR_{sto}}{dTM_{spr}} = \frac{\partial PR_{sto}}{\partial TM_{spr}} + \frac{\partial PR_{sto}}{\partial TM_{sto}} \cdot \frac{dTM_{sto}}{dTM_{spr}} + \frac{\partial PR_{sto}}{\partial TM_{win}} \cdot \frac{dTM_{win}}{dTM_{spr}}$$

$$\frac{dTM_{sto}}{dTM_{spr}} = \frac{\partial TM_{sto}}{\partial TM_{spr}} + \frac{\partial TM_{sto}}{\partial PR_{sto}} \cdot \frac{dPR_{sto}}{dTM_{spr}} + \frac{\partial TM_{sto}}{\partial TM_{win}} \cdot \frac{dTM_{win}}{dTM_{spr}}$$

$$\frac{dTM_{win}}{dTM_{spr}} = \frac{\partial TM_{win}}{\partial TM_{spr}} + \frac{\partial TM_{win}}{\partial PR_{sto}} \cdot \frac{dPR_{sto}}{dTM_{spr}} + \frac{\partial TM_{win}}{\partial TM_{sto}} \cdot \frac{dTM_{sto}}{dTM_{spr}}$$

# SUPPLEMENTARY B

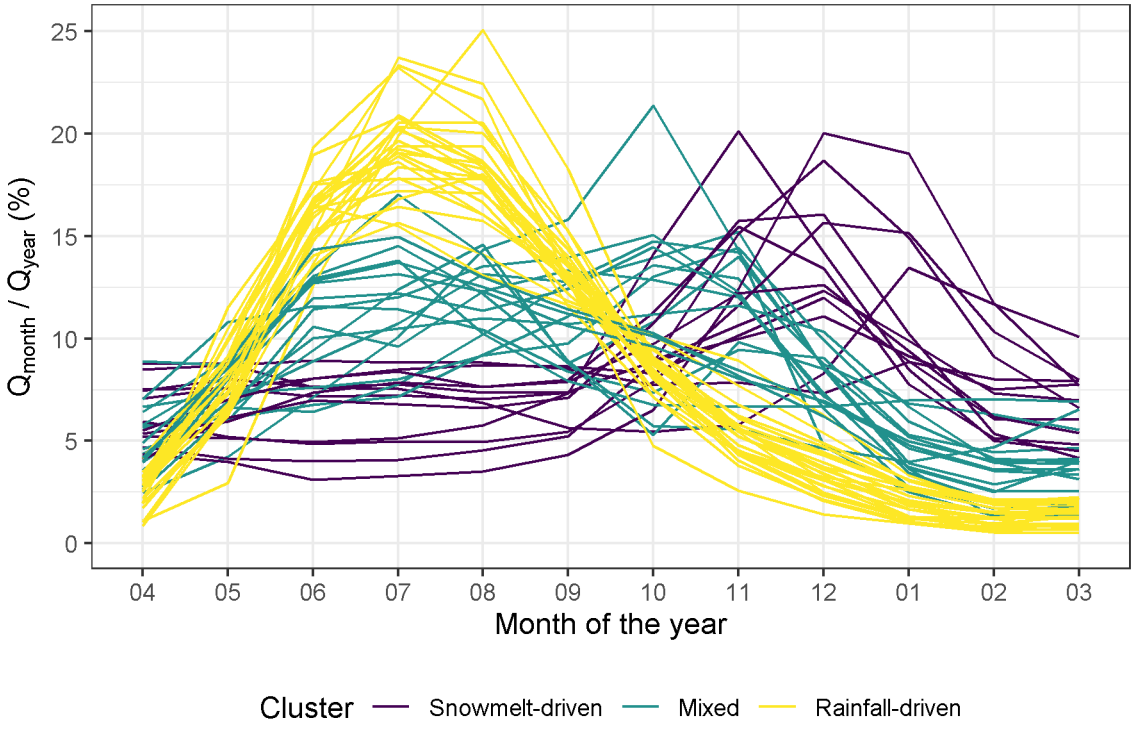


*Figure B-1. For each basin, averaged fractional coefficients of streamflow, as proxies of seasonality. These results are contrasted with the cluster classification procedure, indicating that K-means clustering classification successfully captures the distinct timing regimes.*

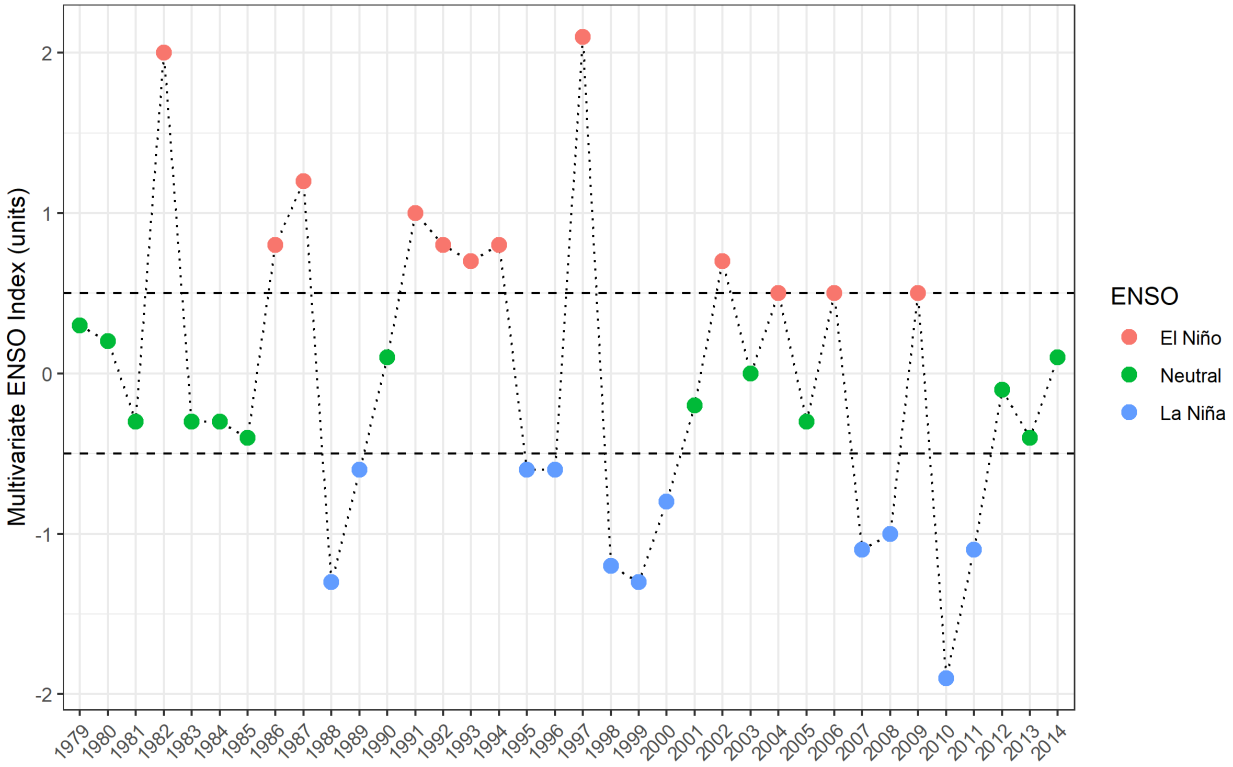


*Figure B-2. Multivariate ENSO Index (MEI) annual time series. For each water year, annual values are calculated as the median of the bimonthly values from https://www.esrl.noaa.gov/psd/enso/mei. Values above 0.5 (below -0.5) were classified as El Niño (La Niña) phase, and neutral otherwise.*

*Table B-1. For each basin, results of the F-test and t-test regarding performance of multiple linear regression models. Bold cells indicate p-value smaller than 5% (95% statistical level of significance). Results for F-test show that all models are significant on their overall performance. On the other hand, results for t-test indicate that $PR_{sto}$ is always significant as predictor; but $TM_{sto}$, $TM_{win}$, and $TM_{spr}$ show varied behavior.*

| Catchment (DGA code) | Cluster classification | F-test (p-value) | t-test (p-value) | | | |
|---|---|---|---|---|---|---|
| | | | $PR_{sto}$ | $TM_{sto}$ | $TM_{win}$ | $TM_{spr}$ |
| 3414001 | Snowmelt-driven | **2.04E-07** | **4.73E-08** | **2.50E-02** | 8.29E-02 | 2.21E-01 |
| 3421001 | Snowmelt-driven | **9.57E-03** | **4.59E-05** | 9.51E-01 | 2.13E-01 | 1.29E-01 |
| 4302001 | Snowmelt-driven | **2.49E-03** | **1.05E-05** | 2.14E-01 | 3.36E-01 | 9.08E-01 |
| 4311001 | Snowmelt-driven | **6.16E-11** | **1.48E-09** | 2.89E-01 | 7.37E-01 | 9.79E-01 |
| 4313001 | Snowmelt-driven | **5.47E-11** | **3.28E-09** | 9.21E-02 | 9.18E-01 | 7.51E-01 |
| 4503001 | Mixed | **1.59E-08** | **6.24E-09** | 5.24E-01 | 5.07E-01 | 2.87E-01 |
| 4513001 | Mixed | **1.49E-51** | **1.31E-15** | 4.52E-01 | 3.95E-01 | 3.72E-01 |
| 4515002 | Mixed | **4.29E-11** | **1.44E-09** | **4.80E-02** | 9.88E-01 | 8.30E-01 |
| 4522002 | Mixed | **2.99E-09** | **1.11E-08** | 3.49E-01 | 2.75E-01 | 3.78E-01 |
| 4531002 | Mixed | **1.42E-09** | **2.53E-09** | 1.39E-01 | 9.54E-01 | 1.65E-01 |
| 4703002 | Snowmelt-driven | **2.19E-58** | **8.22E-16** | **2.57E-02** | 3.49E-01 | 9.66E-01 |
| 5100001 | Mixed | **1.00E-40** | **2.12E-15** | 7.58E-01 | 5.52E-01 | 2.52E-01 |
| 5101001 | Mixed | **6.86E-04** | **4.28E-05** | 4.22E-01 | 3.86E-01 | 2.94E-01 |
| 5200001 | Mixed | **1.30E-11** | **1.82E-09** | 2.42E-01 | 2.41E-01 | 2.69E-01 |
| 5410002 | Snowmelt-driven | **1.46E-48** | **3.74E-15** | 1.13E-01 | 1.08E-01 | 2.73E-01 |
| 5411001 | Mixed | **1.07E-20** | **5.13E-12** | 7.23E-01 | 6.95E-01 | 5.56E-02 |
| 5710001 | Snowmelt-driven | **2.04E-33** | **2.88E-12** | 1.95E-01 | 1.10E-01 | 1.43E-01 |
| 5721001 | Snowmelt-driven | **8.39E-09** | **2.25E-07** | 3.48E-01 | 4.50E-01 | 6.07E-01 |
| 5722001 | Snowmelt-driven | **8.63E-26** | **1.07E-12** | 7.67E-01 | 9.10E-01 | 3.84E-01 |
| 5741001 | Rainfall-driven | **4.76E-32** | **5.22E-14** | **3.59E-02** | 7.23E-01 | **2.66E-03** |
| 6027001 | Mixed | **6.66E-91** | **1.32E-18** | 6.18E-01 | 4.08E-01 | 4.25E-01 |
| 7103001 | Mixed | **8.28E-05** | **5.24E-05** | 1.56E-01 | 4.30E-01 | 3.37E-01 |
| 7112001 | Snowmelt-driven | **7.11E-21** | **1.67E-10** | 8.73E-01 | 6.10E-01 | 1.03E-01 |
| 7115001 | Snowmelt-driven | **8.85E-12** | **1.72E-08** | 4.61E-01 | 6.68E-01 | 2.92E-01 |
| 7330001 | Rainfall-driven | **7.52E-26** | **8.68E-13** | 8.47E-01 | 6.45E-01 | 1.45E-01 |
| 7350003 | Rainfall-driven | **8.51E-48** | **8.28E-15** | 4.19E-01 | 6.47E-01 | 2.31E-01 |
| 7354002 | Rainfall-driven | **5.02E-34** | **8.59E-13** | 5.68E-01 | 5.93E-01 | 4.68E-01 |
| 7358001 | Mixed | **4.29E-12** | **1.96E-09** | **8.50E-03** | **3.60E-03** | 6.71E-02 |
| 7381001 | Mixed | **4.99E-08** | **1.48E-08** | 2.17E-01 | **2.41E-02** | 1.58E-01 |
| 7400001 | Rainfall-driven | **1.14E-05** | **1.01E-07** | 9.56E-01 | 3.13E-01 | 8.76E-01 |
| 8104001 | Mixed | **3.60E-21** | **5.01E-12** | 2.63E-01 | 2.00E-01 | 1.59E-01 |
| 8124001 | Rainfall-driven | **3.21E-52** | **8.65E-17** | 5.77E-01 | 9.46E-01 | 2.15E-01 |
| 8135002 | Rainfall-driven | **1.07E-70** | **2.18E-18** | 7.37E-02 | 3.11E-01 | 6.04E-01 |
| 8220001 | Rainfall-driven | **9.54E-03** | **9.12E-05** | 3.54E-01 | 9.02E-01 | 5.36E-01 |
| 8317002 | Rainfall-driven | **7.82E-25** | **3.43E-13** | 6.48E-01 | 5.11E-01 | 1.53E-01 |
| 8323002 | Rainfall-driven | **2.34E-17** | **2.31E-11** | 2.78E-01 | 1.99E-01 | 1.74E-01 |

| Catchment (DGA code) | Cluster classification | F-test (p-value) | t-test (p-value) | | | |
|---|---|---|---|---|---|---|
| | | | $PR_{sto}$ | $TM_{sto}$ | $TM_{win}$ | $TM_{spr}$ |
| 8330001 | Rainfall-driven | **2.24E-16** | **1.77E-11** | 9.94E-01 | 9.47E-01 | 1.69E-01 |
| 8332001 | Rainfall-driven | **1.48E-27** | **1.80E-13** | 5.85E-01 | 8.62E-01 | 4.11E-01 |
| 8342001 | Rainfall-driven | **1.04E-03** | **4.15E-06** | 9.61E-01 | 9.76E-01 | 2.37E-01 |
| 8343001 | Rainfall-driven | **4.59E-12** | **1.37E-10** | 4.00E-01 | 4.97E-01 | 1.64E-01 |
| 8351001 | Rainfall-driven | **2.10E-08** | **2.94E-09** | 1.78E-01 | 2.83E-01 | 9.05E-02 |
| 8362001 | Rainfall-driven | **9.25E-11** | **5.11E-10** | 6.84E-01 | 8.25E-01 | 7.42E-01 |
| 9102001 | Rainfall-driven | **2.77E-43** | **5.14E-16** | 9.27E-01 | 9.29E-01 | 3.01E-01 |
| 9104002 | Rainfall-driven | **5.44E-10** | **3.63E-10** | 8.02E-01 | 8.68E-01 | 4.79E-01 |
| 9107001 | Rainfall-driven | **1.91E-21** | **6.23E-13** | 7.59E-01 | 7.58E-01 | **4.35E-02** |
| 9123001 | Mixed | **2.57E-07** | **9.20E-08** | 6.53E-01 | 6.07E-01 | **2.25E-02** |
| 9135001 | Rainfall-driven | **3.91E-17** | **1.36E-11** | 1.46E-01 | 7.87E-02 | **4.67E-02** |
| 9404001 | Mixed | **4.10E-21** | **6.12E-11** | **3.94E-02** | 6.21E-02 | **4.04E-02** |
| 9416001 | Mixed | **3.41E-11** | **9.17E-09** | 2.77E-01 | 2.76E-01 | **4.82E-02** |
| 9434001 | Rainfall-driven | **6.44E-17** | **7.19E-12** | 1.03E-01 | 1.16E-01 | 7.20E-02 |
| 9436001 | Rainfall-driven | **2.58E-06** | **4.18E-08** | 8.23E-01 | 8.12E-01 | 2.99E-01 |
| 10134001 | Rainfall-driven | **6.33E-13** | **1.61E-10** | **4.37E-02** | 5.64E-02 | 1.44E-01 |
| 10137001 | Rainfall-driven | **2.18E-05** | **1.01E-07** | 2.73E-01 | 2.01E-01 | 3.41E-01 |
| 10356001 | Rainfall-driven | **6.95E-05** | **1.46E-07** | 9.97E-01 | 5.35E-01 | 7.79E-01 |

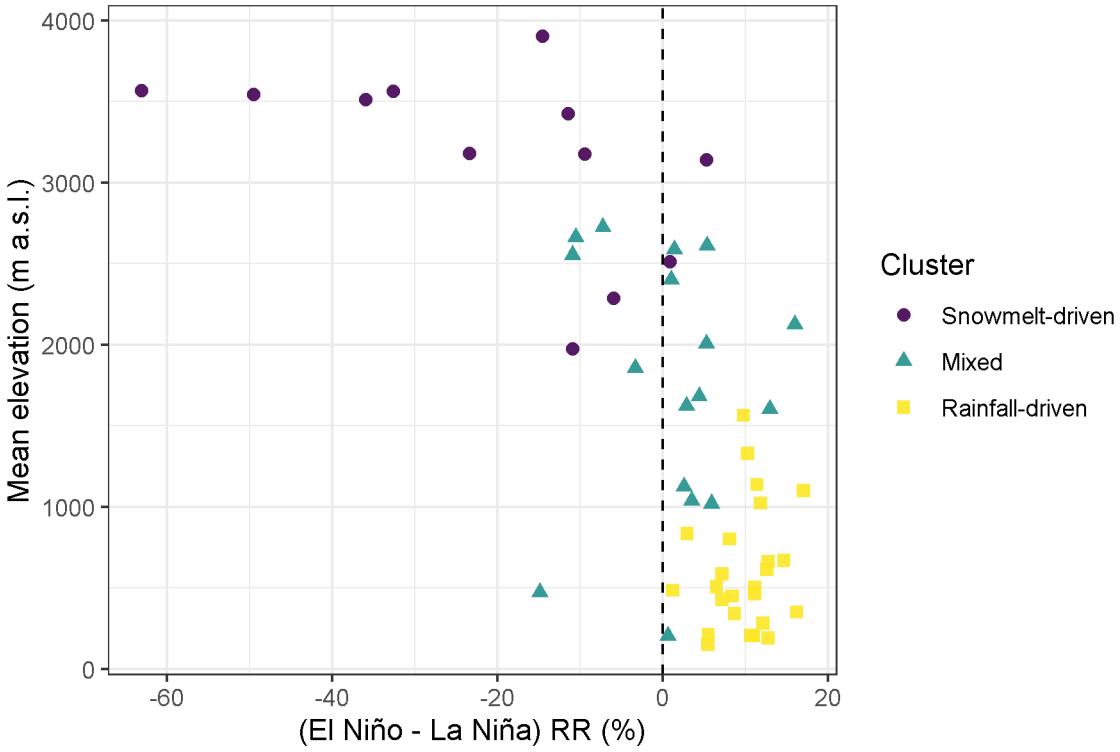


*Figure B-3. Altitudinal control of El Niño minus La Niña composites for annual runoff ratio. Catchments are stratified by cluster classification of hydrologic regimes.*

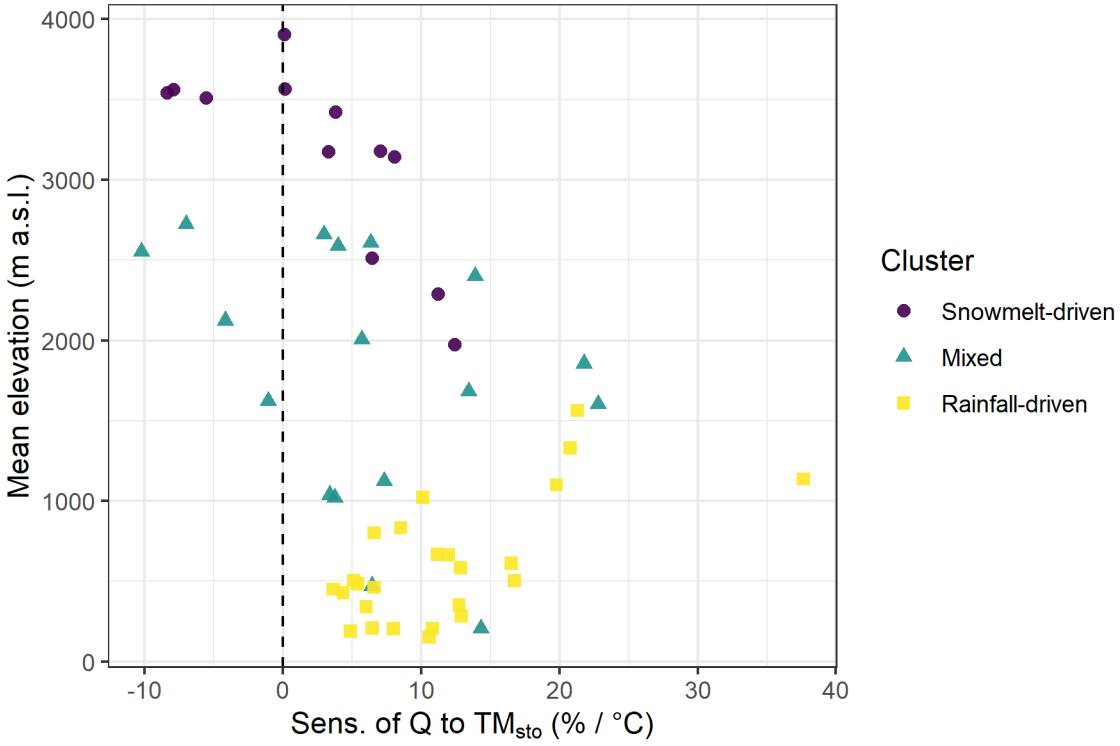


*Figure B-4. Altitudinal control of sensitivity of annual streamflow to mean winter storm temperature. Catchments are stratified by cluster classification of hydrologic regimes.*

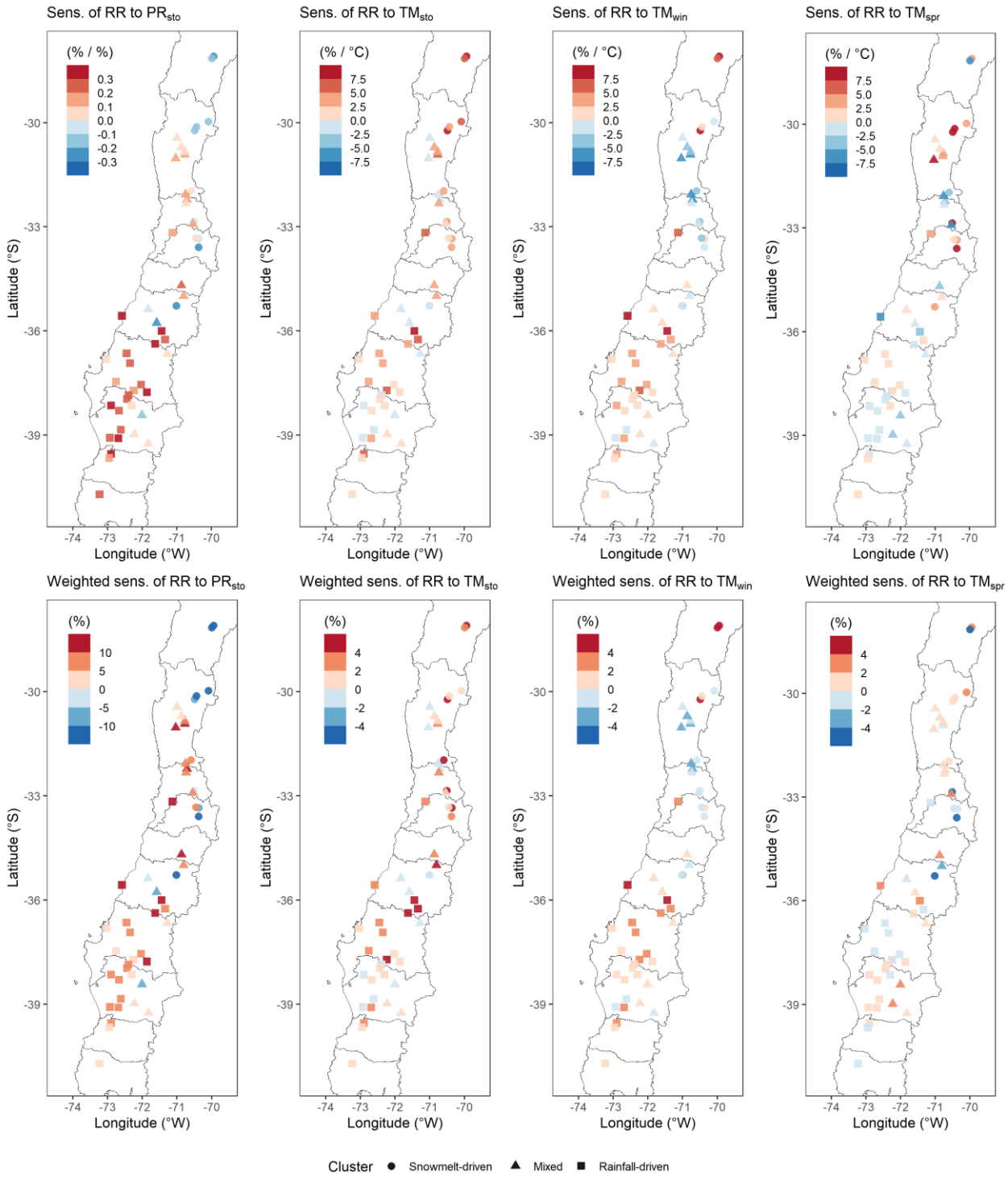


*Figure B-5. (Top panel) Left to right: Sensitivities of annual runoff ratio to winter storm precipitation, winter storm mean temperature, winter mean temperature and spring mean temperature, respectively. (Bottom panel) Same as top but sensitivities are multiplied by El Niño minus La Niña composite anomalies shown at Figure 6. For better visualization, the color palette is truncated at the 5% and 95% percentiles.*